Impact of dust addition on Mediterranean plankton communities under present and future conditions of pH and temperature: an experimental overview

Frédéric Gazeau[1], Céline Ridame[2], France Van Wambeke[3], Samir Alliouane[1], Christian Stolpe[1], Jean-Olivier Irisson[1], Sophie Marro[1], Jean-Michel Grisoni[4], Guillaume De Liège[4], Sandra Nunige[3], Kahina Djaoudi[3], Elvira Pulido-Villena[3], Julie Dinasquet[5,6], Ingrid Obernosterer[6], Philippe Catala[6], Cécile Guieu[1]

[1] Sorbonne Université, CNRS, Laboratoire d'Océanographie de Villefranche, LOV, 06230 Villefranche-sur-Mer, France

[2] CNRS-INSU/IRD/MNHN/UPMC, LOCEAN: Laboratoire d'Océanographie et du Climat: Expérimentation et Approches Numériques, UMR 7159, 75252 Paris Cedex 05, France

[3] Aix-Marseille Université, Université de Toulon, CNRS/INSU, IRD, MIO, UM 110, 13288, Marseille, France

[4] Sorbonne Université, CNRS, Institut de la Mer de Villefranche, IMEV, 06230 Villefranche-sur-Mer, France

[5] Scripps Institution of Oceanography, University of California San Diego, USA

[6] CNRS, Sorbonne Université, Laboratoire d'Océanographie Microbienne, LOMIC, F-66650 Banyuls-sur-Mer, France

Correspondence to: Frédéric Gazeau (f.gazeau@obs-vlfr.fr)

Keywords: Mediterranean Sea; Atmospheric deposition; Plankton community; Ocean acidification; Ocean warming

Abstract

In Low Nutrient Low Chlorophyll areas, such as the Mediterranean Sea, atmospheric fluxes represent a considerable external source of nutrients likely supporting primary production especially during stratification periods. These areas are expected to expand in the future due to lower nutrient supply from sub-surface waters caused by climate-driven enhanced stratification, likely further increasing the role of atmospheric deposition as a source of new nutrients to surface waters. Yet, whether plankton communities will react differently to dust deposition in a warmer and acidified environment remains an open question. The potential impact of dust deposition both in present and future climate conditions was investigated through three perturbation experiments in the open Mediterranean Sea. Climate reactors (300 L) were filled with surface water collected in the Tyrrhenian Sea, Ionian Sea and in the Algerian basin during a cruise conducted in May/June 2017 in the frame of the PEACETIME project. The experimental protocol comprised two unmodified control tanks, two tanks enriched with a Saharan dust analog and two tanks enriched with the dust analog and maintained under warmer (+3 ºC) and acidified (-0.3 pH unit) conditions. Samples for the analysis of an extensive number of biogeochemical parameters and processes were taken over the duration of the experiments (3-4 d). Here, we present the general setup of the experiments and the impacts of dust seeding with and without addressing the effects of environmental changes on nutrients and biological stocks. Dust addition led to a rapid and maximum input of nitrate whereas phosphate release from the dust analog was much smaller. Our results showed that the impacts of Saharan dust deposition in three different basins of the open Northwestern Mediterranean Sea are at least as strong as those observed previously in coastal waters. However, interestingly, the effects of dust deposition on biological stocks were highly different between the three investigated stations and could not be attributed to differences in their degree of oligotrophy but rather to the initial metabolic state of the community. Ocean acidification and warming did not drastically modify the composition of the

47 autotrophic assemblage with all groups positively impacted by warming and acidification.
48 Although autotrophic biomass was more positively impacted than heterotrophic biomass under
49 future environmental conditions, a stronger impact of warming and acidification on
50 mineralization processes suggests a decreased capacity of Mediterranean surface plankton
51 communities to sequester atmospheric CO_2 following the deposition of atmospheric particles.

1. Introduction

Atmospheric deposition is well recognized as a significant source of micro- and macro-nutrients for surface waters of the global ocean (Duce et al., 1991; Jickells et al., 2005; Moore et al., 2013). The potential modulation of the biological carbon pump efficiency and the associated export of carbon by atmospheric deposition events are still poorly understood and quantified (Law et al., 2013). This is especially true for Low Nutrient Low Chlorophyll (LNLC) areas where atmospheric fluxes can play a considerable role in nutrient cycling and that represent 60% of the global ocean surface area (Longhurst et al., 1995) as well as 50% of global carbon export (Emerson et al., 1997). These regions are characterized by a low availability of macronutrients (N, P) and/or metal micronutrients (e.g. Fe) that can severely limit or co-limit phytoplankton growth during large periods of year.

The Mediterranean Sea is a typical example of these LNLC regions and exhibits surface chlorophyll *a* concentrations below 0.2 μg L^{-1} all year round over most of its area, except in the Ligurian Sea where relatively large blooms can be observed in late winter-early spring (e.g. Mayot et al., 2016). Recent assessments showed that the atmospheric input of nutrients in the Mediterranean Sea is of the same order of magnitude as riverine inputs (Powley et al., 2017), making the atmosphere a considerable external source of nutrients (Richon et al., 2018). Atmospheric deposition originates both from natural (mainly Saharan dust) and anthropogenic sources (e.g. Bergametti et al., 1989; Desboeufs et al., 2018). Dust deposition, mostly in the form of pulsed inputs, is mainly associated with wet deposition (Loÿe-Pilot and Martin, 1996). Ternon et al. (2010) reported an average annual dust flux over four years of 11.4 g m^{-2} yr^{-1} (average during the period 2003–2007) at the DYFAMED station in the Northwestern Mediterranean Sea. In this region, the most important events reported in the 2010 decade amounted to ~22 g m^{-2} (Bonnet and Guieu, 2006; Guieu et al., 2010b).

Atmospheric deposition provides new nutrients to the surface waters (Guieu et al., 2010b; Kouvarakis et al., 2001; Markaki et al., 2003; Ridame and Guieu, 2002), Fe (Bonnet and Guieu, 2006) and other trace metals(Desboeufs et al., 2018; Guieu et al., 2010b; Theodosi et al., 2010), that represent significant inputs likely supporting the primary production especially during the stratification period (Bonnet et al., 2005; Ridame and Guieu, 2002), although no clear correlation between dust and ocean color could be evidenced from long series of satellite observation in that part of the basin (Guieu and Ridame, 2020).

Experimental approaches have shown that wet dust deposition events in the Northwestern Mediterranean Sea (the dominant deposition mode in that basin) present a higher impact as a source of bioavailable fertilizing nutrients compared to dry deposition. Indeed, wet deposition provides both new N and P while dry deposition supplies only P and does not allow to stimulate the autotrophic community (except diazotrophs; Ridame et al., 2013), resulting in no increase in chlorophyll *a* concentrations and primary production (Guieu et al., 2014a). This so-called fertilizing effect has been experimentally shown using both micro- and mesocosms where the wet deposition of Saharan dust analog strongly stimulated primary production and phytoplankton biomass (Guieu et al., 2014a; Ridame et al., 2014) while also modifying phytoplankton diversity (Giovagnetti et al., 2013; Lekunberri et al., 2010; Romero et al., 2011). In addition, besides phytoplankton, dust deposition also modified also the bacterial community assemblage and led to even stronger enhancements of production and/or respiration rates (Pulido-Villena et al., 2014). The carbon budget established from four artificial seeding experiments during the DUNE project (Guieu et al., 2014a) showed that by stimulating predominantly heterotrophic bacteria, atmospheric dust deposition can enhance the heterotrophic biological behavior of these oligotrophic waters. This has the potential to reduce the fraction of organic carbon that can be exported to deep waters during the winter mixing period (Pulido-Villena et al., 2008) and ultimately limit net atmospheric CO_2 drawdown.

Another effect induced by Saharan dust deposition is the export of particulate organic carbon (POC), as lithogenic particles can aggregate and ballast dissolved organic matter (Bressac et al., 2014; Desboeufs et al., 2014; Louis et al., 2017a; Ternon et al., 2010). This so-called lithogenic carbon pump can represent a major part of the carbon export following a dust deposition event (up to 50% during the DUNE experiment; Bressac et al., 2014). Recently, Louis et al. (2017a) showed that Saharan dust deposition triggers the abiotic formation of transparent exopolymeric particles (TEP), leading to the formation of organic-mineral aggregates, a formation process that is highly dependent on the quality and quantity of TEP-precursors initially present in seawater.

In response to ocean warming and increased stratification, nutrient cycling in the open ocean is being and will continue to be perturbed in the next decades resulting very likely in regionally variable impacts (IPCC, 2019). Overall, LNLC areas are expected to expand in the future (Irwin and Oliver, 2009; Polovina et al., 2008) due to a thermal stratification related reduction of nutrients supply from sub-surface waters (Behrenfeld et al., 2006). As such, the role of atmospheric deposition might increase as an alternative source of new nutrients to surface waters. Ongoing warming and acidification of the global ocean (IPCC, 2019) are also evidenced in the Mediterranean Sea (e.g. Kapsenberg et al., 2017; The Mermex group, 2011). Whether or not plankton communities will respond differently to dust deposition in future conditions is still largely unknown. Although dependent on resource availability, it is well known that remineralisation by bacteria is subject to positive temperature control (López-Urrutia and Morán, 2007). As under severe nutrient limitation, warming has no effect on primary productivity (Marañón et al., 2018), it will most likely further push the balance towards net heterotrophy in oligotrophic areas.

With respect to ocean acidification, an *in situ* mesocosm experiment conducted during the summer stratified period in the Northwestern Mediterranean Sea showed that the plankton

community was rather insensitive to this perturbation under strong nutrient limitation (Maugendre et al., 2017, and references therein). This is coherent with results from Maugendre et al. (2015), based on a batch experiment, showing that, under nutrient-depleted conditions in late winter, ocean acidification has a very limited impact on the plankton community and that small species (e.g. Cyanobacteria) might benefit from warming with a potential decrease of the export and energy transfer to higher trophic levels. In contrast, in more eutrophic coastal conditions, Sala et al. (2016) showed that ocean acidification exerted a positive effect on phytoplankton, especially on pico- and nano-phytoplankton. Similarly, Neale et al. (2014) showed in a coastal ecosystem of the Alboran Sea that ocean acidification could lead, although moderately, to high chlorophyll levels under low light conditions with an opposite effect under high irradiance.

To date and to the best of our knowledge, there have been no attempts to evaluate the behavior of plankton communities after the deposition of atmospheric particles in the context of future levels of temperature and pH. Yet, following the recommendation from Maugendre et al. (2017), any perturbation experiment for future climate conditions in the Mediterranean Sea should consider atmospheric deposition as a source of new nutrients and consider both temperature and pH as external forcings. Such experiments were conducted in the frame of the PEACETIME project (ProcEss studies at the Air-sEa Interface after dust deposition in the MEditerranean sea; http://peacetime-project.org/) during the cruise on board the R/V "Pourquoi Pas?" in May/June 2017. The project aimed at extensively studying and parameterizing the chain of processes occurring in the Mediterranean Sea after atmospheric deposition and to put them in perspective of on-going environmental changes (Guieu et al., 2020). During that cruise, three perturbation experiments were conducted in climate reactors (300 L tanks) filled with surface water collected in the Tyrrhenian Sea (TYR), Ionian Sea (ION) and in the Algerian basin (FAST; Fig. 1). Six tanks were used to follow simultaneously and with a high temporal resolution, the evolution of biological activity and stocks, nutrients stocks, dissolved organic matter as well as

151 particles dynamics and export, following a dust deposition event simulated at their surface, both
152 under present environmental conditions and following a realistic climate change scenario for
153 2100 (ca. +3 °C and -0.3 pH units; IPCC, 2013). In this manuscript, we will present the general
154 setup of the experiments and the evolution of nutrient and biological stocks (heterotrophic and
155 autotrophic prokaryotes, photosynthetic eukaryotes as well as micro- and meso-zooplankton).
156 Several other manuscripts, related to these experiments and currently submitted to or published
157 in this special issue, focus on plankton metabolism (primary production, heterotrophic
158 prokaryote production) and carbon export (Gazeau et al., 2021), on the microbial food web
159 (Dinasquet et al., 2021), on nitrogen fixation (Céline Ridame, unpublished results) and on the
160 release of insoluble elements (Fe, Al, REE, Th, Pa) from dust (Roy-Barman et al., 2020).

2. Material and Methods

2.1. General setup

Six experimental tanks (300 L; Fig. 2), in which the irradiance spectrum and intensity can be finely controlled and in which future ocean acidification and warming conditions can be fully reproduced, were installed in a temperature-controlled container. The tanks are made of high-density polyethylene (HDPE) and are trace-metal free in order to avoid contaminations, with a height of 1.09 m, a diameter of 0.68 m, a surface area of 0.36 m^2 and a volume of 0.28 m^3. All tanks were cleaned before the experimental work following the protocol described by Bressac and Guieu (2013). A weak turbulence was generated by a rotating PVC blade (9 rpm) in order to mimic natural conditions. Each tank was equipped with a lid containing six rows of LEDs (Alpheus©). Each of these rows were composed of blue, green, cyan and white units in order to mimic the natural sun spectrum. At the conical base of each tank, a polyethylene (PE) bottle collecting the exported material from above was screwed onto a polyvinyl chloride (PVC) valve that remained open during the duration of the whole experiment. Photosynthetically active radiation (PAR; 400-700 nm) and temperature were continuously monitored in each tank using respectively QSL-2100 Scalar PAR Irradiance Sensors (Biospherical Instruments©) and pt1000 temperature sensors (Metrohm©) connected to a D230 datalogger (Consort©).

The experimental protocol comprised two unmodified control tanks (C1 and C2), two tanks enriched with Saharan dust (D1 and D2) and two tanks enriched with Saharan dust and maintained under warmer (+3 ºC) and acidified (-0.3 pH unit) conditions (G1 and G2). The atmosphere above tanks C1, C2, D1 and D2 was flushed with ambient air (ca. 400 ppm, 6 L min^{-1}) and tanks G1 and G2 were flushed with air enriched with CO_2 (ca. 1000 ppm, 6 L min^{-1}) in order to prevent CO_2 degassing from the acidified tanks. CO_2 partial pressure (pCO_2) in both

ambient air and CO_2-enriched air was monitored using two gas analysers (LI-820, LICOR©). The CO_2 concentration in the CO_2-enriched air was manually controlled through small injections of pure CO_2 (Air Liquide©) using a mass flow controller.

Three experiments were performed at the long duration stations TYR, ION and FAST. The tanks were filled by means of a large peristaltic pump (Verder© VF40 with EPDM hose, flow of 1200 L h^{-1}) collecting seawater below the base of the boat (depth of ~ 5 m), used to supply continuously surface seawater to a series of instruments during the entire campaign. In order to homogeneously fill the tanks, the flow was divided into six HDPE pipes distributing the water simultaneously into the different tanks. Overall, the filling of the six tanks took ~2 h (including rinsing and initial sampling, see thereafter). At the three stations, tanks were always filled at the end of the day before the start of the experiments: TYR (17/05/2017), ION (25/05/2017) and FAST (02/06/2017). While filling the tanks, this surface seawater was sampled for the measurements of selected parameters (sampling time = t-12h before dust seeding, see Table 1). After filling the tanks, seawater was slowly warmed using 500 W heaters, controlled by temperature-regulation units (COREMA©), in G1 and G2 overnight to reach an offset of +3 °C. ^{13}C-bicarbonate was added to all tanks at 4:00 am (local time; Gazeau et al., 2021) and G1 and G2 were acidified by addition of CO_2-saturated filtered (0.2 µm) seawater (~1.5 L in 300 L; collected when filling the tanks at each station) at 4:30 am to reach a pH offset of -0.3. Sampling for most parameters took place prior to dust seeding (sampling time = t0, see Table 1). Dust seeding was performed right after t0 between 7:00 and 9:00 (local time) in tanks D1, D2, G1 and G2. The same dust analog was used and the same dust flux was simulated as for the DUNE 2009 experiments described in Desboeufs et al. (2014). Briefly, the fine fraction (< 20 µm) of Saharan soils collected in southern Tunisia, which is a major source of dust deposition over the northwestern Mediterranean basin, was used in the seeding experiments. The particle size distribution showed that 99% of particles had a size smaller than 0.1 µm, and that particles were

mostly made of quartz (40%), calcite (30%) and clay (25%; Desboeufs et al., 2014). This collected dust underwent an artificial chemical aging process by addition of nitric and sulfuric acid (HNO_3 and H_2SO_4, respectively) to mimic cloud processes during atmospheric transport of aerosol with anthropogenic acid gases (Guieu et al., 2010a, and references therein). To mimic a realistic wet flux event of 10 g m^{-2}, 3.6 g of this analog dust were quickly diluted into 2 L of ultrahigh-purity water (UHP water; 18.2 MΩ cm^{-1} resistivity), and sprayed at the surface of the tanks using an all-plastic garden sprayer (duration = 30 min). The N and P total contents in the dust were 1.36 ± 0.09% of N and 0.055 ± 0.003% of P (see Desboeufs et al., 2014, for a full description of dust chemical composition). The experimental protocol included the analysis of an extensive number of biogeochemical parameters and processes, not all shown and discussed in this paper, and are listed in Table 1. The experiment at stations TYR and ION lasted 72 h (3 days) whereas the last experiment at station FAST was extended to four days. This relatively short duration of the experiments was constrained by the time available between stations and the time needed to properly clean the tanks between the experiments, following the protocol described by Bressac and Guieu (2013). As a larger time window was possible at the end of the cruise, the experiment at FAST was extended to four days. Seawater sampling was conducted 1 h (t1h), 6 h (t6h), 12 h (t12h), 24 h (t24h), 48 h (t48h) and 72 h (t72h) (+ 96 h = t96h for station FAST) after dust addition. Acid-washed silicone tubes were used for transferring the water collected from the tanks to the different vials or containers. For some parameters (e.g. micro- and macro-nutrients), sampled seawater was directly filtered at the exit of the sampling tubes connected to each tank on sterile membrane filter capsules (gravity filtration with Sartobran© 300; 0.2 μm).

2.2. Analytical methods

2.2.1. Carbonate chemistry

Seawater samples for pH measurements were stored in 300 mL glass bottles with a glass stopper, pending analysis on board (within 2 h). Samples were transferred to 30 mL quartz cells and absorbances at 434, 578 and 730 nm were measured at 25 °C on an Cary60 UV-Spectrophotometer (Agilent©) before and after addition of 50 µL of purified meta-cresol purple provided by Robert H. Byrne (University of South Florida, USA) following the method described by Dickson et al. (2007). pH on the total scale (pH_T) was computed using the formula and constants of Liu et al. (2011). The accuracy of pH measurements was estimated to 0.007 pH units, using a TRIS buffer solution (salinity 35, provided by Andrew Dickson, Scripps university, USA).

Seawater samples for total alkalinity (A_T; 500 mL) measurements were filtered on GF/F membranes and analyzed onboard within one day. A_T was determined potentiometrically using a Metrohm© titrator (Titrando 888) and a glass electrode (Metrohm©, ecotrode plus) calibrated using first NBS buffers (pH 4.0 and pH 7.0, to check that the slope was Nernstian) and then using a TRIS buffer solution (salinity 35, provided by Andrew Dickson, Scripps university, USA). Triplicate titrations were performed on 50 mL sub-samples at 25 ºC and A_T was calculated as described by Dickson et al. (2007). Titrations of standard seawater provided by Andrew Dickson (Scripps university, USA; batch 151) yielded A_T values within 5 µmol kg^{-1} of the nominal value (standard deviation = 1.5 µmol kg^{-1}, n = 40).

All parameters of the carbonate chemistry were determined from pH_T, A_T, temperature, salinity, as well as phosphate and silicate concentrations using the R package seacarb. Propagation of errors on computed parameters was performed using the new function “error” of

this package, considering errors associated with the estimation of A_T, pH_T as well as errors on dissociation constants (Orr et al., 2018).

2.2.2. Nutrients

Seawater samples for dissolved nutrients were filtered directly at the exit of the sampling tubes connected to each tank (Sartobran© 300; 0.2 µm), collected in polyethylene bottles and immediately analyzed on board. Nitrate + nitrite (NO_x) and silicate ($Si(OH)_4$) measurements were conducted using a segmented flow analyzer (AAIII HR Seal Analytical©) according to Aminot and Kérouel (2007) with a limit of quantification of 0.05 µmol L^{-1} for NO_x and 0.08 µmol L^{-1} for $Si(OH)_4$. In addition, for t-12h samples, the analysis of NO_x was also performed by a spectrometric method in the visible at 540 nm, with a 1 m Liquid Waveguide Capillary Cell (LWCC). The limit of detection was ~10 nmol L^{-1} and the reproducibility was ~6%. Also from samples taken at t-12h, the measurement of ammonium concentrations was performed on board using a Fluorimeter TD-700 (Turner Designs©) according to Holmes et al. (1999). This fluorimetric method is based on the reaction of ammonia with orthophtaldialdehyde and sulfite and has a limit of quantification of 0.01 µmol L^{-1}. Dissolved inorganic phosphorus (DIP) concentrations were quantified using the Liquid Waveguide Capillary Cell (LWCC) method according to Pulido-Villena et al. (2010). The LWCC was 2.5 m long and the limit of detection was 1 nmol L^{-1}.

2.2.3. Pigments

A volume of 2.5 L of sampled seawater was filtered onto GF/F filters, immediately frozen in liquid nitrogen and stored at -80 ºC pending analysis at the SAPIGH analytical platform at the Institut de la Mer de Villefranche (IMEV, France). Filters were extracted at -20 ºC in 3 mL methanol (100%) containing an internal standard (vitamin E acetate, Sigma©), disrupted by

sonication and clarified one hour later by vacuum filtration through GF/F filters. The extracts were rapidly analyzed (within 24 h) on a complete Agilent© Technologies 1200 series HPLC system. The pigments were separated and quantified as described in Ras et al. (2008).

2.2.4. Flow cytometry

For the enumeration of autotrophic prokaryotic and eukaryotic cells, heterotrophic prokaryotes and heterotrophic nanoflagellates (HNF) by flow cytometry, subsamples (4.5 mL) were fixed with glutaraldehyde grade I 25% (1% final concentration), and incubated for 30 min at 4 °C, then quick-frozen in liquid nitrogen and stored at -80 °C until analysis. Samples were thawed at room temperature. Counts were performed on a FACSCanto II flow cytometer (Becton Dickinson©) equipped with 3 air-cooled lasers: blue (argon 488 nm), red (633 nm) and violet (407 nm). The separation of different autotrophic populations was based on their scattering and fluorescence signals according to Marie et al. (2010). *Synechococcus* spp. was discriminated by its strong orange fluorescence (585 ± 21 nm), and pico- and nano-eukaryotes were discriminated by their scatter signals of red fluorescence (> 670 nm). For the enumeration of heterotrophic prokaryotes, cells were stained with SYBR Green I (Invitrogen – Molecular Probes) at 0.025% (vol / vol) final concentration for 15 min at room temperature in the dark. Stained prokaryotic cells were discriminated and enumerated according to their right-angle light scatter (SSC) and green fluorescence at 530/30 nm. In a plot of green versus red fluorescence, heterotrophic prokaryotes were distinguished from autotrophic prokaryotes. For the enumeration of HNF, staining was performed with SYBR Green I (Invitrogen—Molecular Probes) at 0.05% (v/v) final concentration for 15-30 min at room temperature in the dark (Christaki et al., 2011). Cells were discriminated and enumerated according to their SSC and green fluorescence at 530/30 nm. Fluorescent beads (1.002 µm; Polysciences Europe©) were systematically added to each analyzed sample as internal standard. The cell abundance was determined from the flow rate,

which was calculated with TruCount beads (BD biosciences©). Biomasses of each group were estimated based on conversion equations and/or factors found in the literature (see section 2.3.2).

2.2.5. Micro-phytoplankton and -heterotrophs

At t-12h (i.e. seawater sampled during the filling of the tanks), a volume of 500 mL was sampled in glass vials and immediately preserved in a 5% acidic Lugol's solution pending analysis. At the Laboratoire d'Océanographie de Villefranche (LOV, France), 100 mL aliquots were transferred to sedimentation chambers (Utermohl) and counted under an inverted microscope at 200 to 400 magnifications.

2.2.6. Mesozooplankton

At the end of each experiment (t+72h for TYR and ION and t+96 h for FAST, after artificial dust seeding), the sediment traps were removed, closed and stored with formaldehyde 4% (see Gazeau et al., 2021). The valve at the base of the tanks was then reopened to let the remaining water inside the tanks (TYR 165-180 L; ION = 172.5 L and FAST = 150 L) pass through a large PVC sieve (100 µm). The organisms retained on that mesh were gently removed from the sieve using a washing bottle filled with filtered seawater (0.2 µm), and transferred directly inside a 250 mL bottle. The bottle was filled with the sample (1/3 of the volume), and was completed with formaldehyde 4%. The zooplankton digital images were obtained using a ZooSCAN (Hydroptic©; Gorsky et al., 2010) at the PIQv-platform of EMBRC-France. The identification of species was performed by automatic classification with a reference dataset in EcoTaxa (https://ecotaxa.obs-vlfr.fr/, last access: 17/04/2020) and then all validated and corrected manually.

2.3. Data analyses

2.3.1. Nutrient inputs from dust

The maximum percentage of dust-born dissolved N and P was calculated considering that these evapo-condensated dust contain 1.36 ± 0.09% of N and 0.055 ± 0.003% of P (Desboeufs et al., 2014). Based on maximal concentrations observed in the D and G tanks after seeding (two discrete sampling within 6 h following dust seeding, t1h and t6h), one can estimate the maximal % of dissolution of dust in seawater during the three experiments:

$$\%_{dissolution} = \frac{CONC_{max} - CONC_{init}}{CONC_{dust}} . 100 \quad (1)$$

where $CONC_{init}$ is the concentration of the corresponding nutrient in each tank before seeding (t0), $CONC_{max}$ corresponds to the concentration of the corresponding nutrient in each tank when nutrient concentration was at a maximum over the first 6 h after seeding as observed based on our discrete sampling procedure, and $CONC_{dust}$ is the maximum addition, corresponding to a 100% dissolution of its total concentration in the dust analog (as estimated based on dust chemical composition; Desboeufs et al., 2014; see above).

2.3.2. Autotrophic and heterotrophic biomass

As micro-phytoplankton counting was not performed throughout the experiment, as a first approximation, autotrophic biomass was calculated as the sum of carbon contained in *Synechococcus*, pico-eukaryotes and nano-eukaryotes (abundances based on flow cytometry) and is therefore restricted to the fraction < 20 µm. For *Synechococcus*, conversion to carbon units was done considering 250 fg C $cell^{-1}$ (Kana and Glibert, 1987), while the equation proposed by Verity et al. (1992; 0.433 $BV^{0.863}$ where BV refers to the biovolume) was used for pico- and nano-eukaryotes assuming a spherical shape and a diameter of 2 and 6 µm for the two groups,

respectively. Percentages of these different groups were calculated in order to estimate the composition of the communities at the start and its evolution during the experiments. Furthermore, heterotrophic biomass was computed as the sum of heterotrophic prokaryotes biomass and heterotrophic nanoflagellates biomass. For heterotrophic prokaryotes, conversion to carbon units were done considering 20 fg C $cell^{-1}$ (Lee and Fuhrman, 1987) and for heterotrophic nanoflagellates assuming 220 fg C μm^{-3} (Børsheim and Bratbak, 1987), a spherical shape and a diameter of 3 μm. The ratio of autotrophic and heterotrophic biomass during the experiments was used to evaluate the trophic status of the investigated communities and its evolution. Finally, a proxy for micro-phytoplankton biomass (B_{micro}) was estimated following Vidussi et al. (2001), as the sum of Fucoxanthin and Peridinin.

3. Results

3.1. Initial conditions

Initial conditions of various measured parameters at the three sampling stations while filling the tanks (t-12h before seeding) are shown in Table 2. pH_T and total alkalinity concentrations followed a west to east increasing gradient (8.03, 8.04 and 8.07; 2443, 2529 and 2627 µmol kg^{-1} at FAST, TYR and ION, respectively). NO_x concentrations were maximal at station FAST with a NO_x:DIP molar ratio of ~ 4.6. Very low NO_x concentrations were observed at stations TYR and ION (14 and 18 nmol L^{-1}, respectively). DIP concentrations were the highest at station TYR (17 nmol L^{-1}) and the lowest at the most eastern station (ION, 7 nmol L^{-1}). Consequently, the lowest NO_x:DIP ratio was measured at TYR (0.8), compared to ION and FAST (2.8 and 4.6, respectively). Ammonium concentrations were maximal at TYR (0.045 µmol L^{-1}), intermediate at ION (0.022 µmol L^{-1}), and minimal at FAST (below detection limit). Silicate concentrations were similar at stations TYR and ION (~ 1 µmol L^{-1}) and higher than at station FAST (0.64 µmol L^{-1}).

Very low and similar concentrations of chlorophyll *a* were measured at the three stations (0.063 - 0.072 µg L^{-1}). The proportion of the different major pigments (Fig. 3) showed that phytoplankton communities at stations TYR and ION were very similar with a dominance of Prymnesiophytes (i.e. 19'-hexanoyloxyfucoxanthin; Ras et al., 2008) followed by Cyanobacteria (i.e. Zeaxanthin; Ras et al., 2008). In contrast, at station FAST, the plankton community was clearly dominated by photosynthetic prokaryotes (i.e. Zeaxanthin and Divinyl-chlorophyll a; Cyanobacteria and Prochlorophytes, respectively; Ras et al., 2008). At all three stations, the proportion of pigments representative of larger species (i.e. Fucoxanthin and Peridinin; diatoms and dinoflagellates respectively; Ras et al., 2008) were very small (< 5% for each pigment).

Cellular abundances of all studied microorganisms (phytoplankton, micro-grazers, heterotrophic bacteria) were the highest at FAST (Table 2). Picoeukaryotes, *Synechococcus* and heterotrophic prokaryotes abundances followed an east to west increasing trend (ION < TYR < FAST). In contrast, nano-eukaryotes abundance was similar at FAST and ION, and minimal at TYR. The abundance of heterotrophic nanoflagellates (HNF) were similar at TYR and FAST (~110-125 cells mL^{-1}), twice as high as the one observed at station ION. This east to west increasing trend was also observed for micro-phytoplankton and micro-heterotrophs abundances (microscopic analyses; Table 2). The ratio between autotrophic biomass and heterotrophic biomass was clearly in favor of the heterotrophic compartment at stations TYR and FAST (~0.6 at the two stations) but the opposite was found at station ION (ca. 1.3).

3.2. Conditions of irradiance, temperature and pH during the experiments

Irradiance levels, during the experiments in the control tanks (C1, C2), were maximal at station ION and minimal at station FAST (daily average maximum levels in controls: ~ 1050, ~ 1130 and ~ 1020 µmol photons m^{-2} s^{-1} at TYR, ION and FAST, respectively; Fig. 4). Decreases of water transparency after dust addition was observed at all three stations with a maximum dust impact at station ION and the lowest impact at station FAST where irradiance levels decreased by only 60 µmol photons m^{-2} s^{-1} after dust addition (average between tanks D and G). At station TYR, a more pronounced decrease was observed in acidified and warmed tanks (G1 and G2) with a decrease of daily average maximum irradiance of ~ 60 and ~ 160 µmol photons m^{-2} s^{-1} as compared to dust-amended tanks D and controls, respectively. Temperature control (Fig. 4) was not optimal showing deviations between replicates of treatment G of up to 1.5 °C (station ION). Temperature in controls and D tanks displayed a daily cycle with an increase during the day and

a decrease at night. Overall, the differences between the warmed treatment (G) and the other tanks were +3, +3.2 and +3.6 °C at TYR, ION and FAST, respectively.

Addition of CO_2-saturated filtered seawater led to a decrease of pH_T from 8.05 ± 0.004 (average ± SD between C1, C2, D1 and D2 at t0) to 7.74 (average between G1 and G2) at station TYR, from 8.07 ± 0.002 to 7.78 at station ION and 8.05 ± 0.001 to 7.72 at station FAST (Fig. 5). pH_T levels remained more or less constant in ambient pH levels tanks during all three experiments with no clear impact of dust addition in tanks D1 and D2. In lowered pH tanks, pH levels gradually increased during the experiments with a systematic larger increase in one of the duplicates (G1). Yet pH_T increases remained moderate thanks to the flushing of CO_2-enriched air above the tanks (pCO_2 of 1017 ± 11, 983 ± 96, 1023 ± 25 ppm at TYR, ION and FAST, respectively; data not shown). Partial pressure of CO_2 in ambient air was similar at the three stations, i.e. 410 ppm (data not shown). At all three stations, the addition of ^{13}C-bicarbonate to all tanks before t0 led to an increase of total alkalinity between 6 and 11 µmol kg^{-1} at t0. Dust addition, performed right after t0 in tanks D and G, led to a A_T decrease in these tanks between 8 and 16 µmol kg^{-1} at t24h with no apparent effects of warming and acidification. Overall, no large changes in this parameter were observed during the experiments (Fig. 5).

3.3. Changes in nutrient concentrations

Dust addition in tanks D and G led to a rapid and maximum input of NO_x (as observed during the first 6 h; Fig. 6; Table 3) of ~ 11 µmol L^{-1} at all three stations with no differences between both treatments. The corresponding dissolution percentage of N contained in the dust analog was between 94 and 99%. In contrast, maximum DIP release (within 6 h after dust addition) from the dust analog was much smaller and comprised between 20 and 37 nmol L^{-1}, with slightly higher release at FAST (31-37 nmol L^{-1}) as compared to the other stations. Dissolution percentages for DIP were estimated between 9.2 and 17.3% of total phosphorus

424 contained in dust. As a consequence of these contrasted dissolution of N and P, NO_x:DIP ratios
425 increased from initial values below 5 to above 300, within 6 h after dust seeding, in the dust
426 amended (D and G) tanks (Fig. 6).

427 After these rapid increases due to N and P releases in dust amended tanks, both variables
428 decreased with time. While nutrient variability was small in control tanks over the duration of the
429 experiments (NO_x and DIP variations below 20 and 3 nmol L^{-1}, respectively), large decrease of
430 both elements was measured in dust amended tanks (D and G; Table 4). For NO_x, similar linear
431 decreases were observed throughout the experiments at stations TYR and ION with no visible
432 differences between tanks D and G. In contrast, at station FAST, a more pronounced decrease in
433 NO_x was observed in dust-amended (D and G) tanks as compared to the other stations, with
434 detectable larger decreases in warmed and acidified tanks relative to the D treatment.
435 Nevertheless, at all stations, NO_x concentrations in D and G treatments remained far above
436 ambient levels throughout the experiments (> 9 μmol L^{-1}). Abrupt decreases in DIP were
437 observed during the three experiments after the initial increase. At station TYR, after 24 h, all
438 DIP released from dust decreased to initial levels in tanks G while it took two more days to reach
439 initial levels in tanks D. In contrast, at station ION, no clear difference in DIP dynamics was
440 observed between treatments D and G, with concentrations that decreased rapidly during the first
441 24 h but that remained above initial levels until the end of the experiment. At station FAST,
442 similarly to station TYR, DIP decreased rapidly from t12h in treatment G, reaching levels close
443 to initial conditions at the end of the experiment. DIP decrease was much lower in treatment D
444 (Table 4) with concentrations maintained far above ambient levels throughout the experiment.
445 As a consequence of these differences between NO_x and DIP dynamics as well as differences
446 among stations, NO_x:DIP ratio increased during the experiments with clear differences between
447 stations (Fig. 6) and remained much higher than that in the controls over the duration of the three
448 experiments.

Silicate dynamics showed at all stations higher concentrations in dust amended (D and G) tanks relative to the controls. At TYR, while concentrations remained stable in control tanks, they increased linearly with time in the other tanks (D and G) with no apparent effect of the imposed increase in temperature and decrease in pH (i.e. tanks G). Difference of $Si(OH)_4$ concentration between dust amended treatments (D and G) and controls was ~0.1 µmol L^{-1} at the end of the experiment. At station ION, after an initial decrease of concentrations between t-12h and t0, concentrations increased in all tanks until the end of the experiment with higher concentration in dust amended tanks (D and G) than in controls (no difference between D and G treatments). In contrast, at FAST, concentrations increased between t-12h and t0, and continued to increase in all tanks (with higher values in dust amended tanks) until t48h and then decreased until the end of the experiment. At the end of the experiment (t96h), $Si(OH)_4$ concentration was higher in the G treatment than in the D treatment which was similar to the controls.

3.4. Changes in biological stocks

Regarding biological stocks, temporal dynamics showed very different patterns amongst the three studied stations. At TYR, total chlorophyll *a* concentrations did not change in dust amended tanks maintained under ambient levels of temperature and pH (Fig. 7) and even led to slightly decreased values 24 h after dust addition (e.g. -35 to -38% in D1 and D2, respectively as compared to controls; Table 5). No clear effect of dust addition (tanks D vs. C) were detectable for all groups based on pigment analyses (Fig. 7). Results obtained based on flow cytometry counting (Fig. 8) were coherent with these observations and showed stronger decreases in cell abundances for < 20 µm autotrophic groups in tanks D1 and D2 (-77 to -80%). In contrast, at this station, the abundance of heterotrophic prokaryotes (HP) increased rapidly after dust addition both under ambient (+53-68%) and future (+68%) environmental conditions, with no clear difference among those treatments. In warmed and acidified tanks, strong discrepancies between

473 the duplicates were observed for pigments and autotrophic cell abundances. Indeed, tank G1
474 showed moderately higher levels for all variables as compared to tanks C with the exception of
475 pico-eukaryotes, while in G2 all variables responded strongly to dust addition with maximum
476 relative changes of > 300% (with the exception of nano-eukaryotes: +119%). While HNF
477 abundances responded positively to the treatments in D1, D2 and G2 (+100-352%), abundances
478 increased sharply in tank G1 towards the end of the experiment (+1095%).

479 At ION, a clear distinction between treatments could be observed for almost all pigments
480 and cell abundances (Fig. 7, Fig. 8). With the exception of nano-eukaryotes and HNF, all
481 variables (pigments and cell abundances) increased as a response to both dust addition and
482 warmed/acidified conditions (i.e. C < D < G). As an example (Table 5), the maximum relative
483 changes as compared to controls observed for total chlorophyll *a* were 109-183% and 399-426%
484 in tanks D and G, respectively. The highest stimulation to dust addition was observed for
485 *Synechococcus* with a +317-390% increase and +805-1425% increase in D and G tanks
486 respectively (Table 5). Abundances of nano-eukaryotes and HNF suggested no impact of dust
487 addition under ambient conditions but a positive impact in treatment G. In contrast to what was
488 observed at TYR for HP abundances, an effect of temperature and pH was observed at station
489 ION with a higher impact of dust addition under future environmental conditions.

490 At station FAST, all above mentioned variables related to biological stocks increased
491 strongly after dust addition (Fig. 7, Fig. 8 and Table 5). For instance, total chlorophyll *a*
492 increased following an exponential trend until the end of the experiment reaching maximal
493 values at t96h with slightly lower values observed under ambient environmental conditions
494 (+237-318% in D tanks vs. ~ +400% in G tanks). Prymnesiophytes (i.e. 19'-
495 hexanoyloxyfucoxanthin) and diatoms (i.e. Fucoxanthin) appeared as the groups benefiting the
496 most from dust addition with no large impacts of warming/acidification. In contrast,
497 Pelagophytes (i.e. 19'-butanoyloxyfucoxanthin) and green algae (i.e. Total Chlorophyll *b*)

responded much more in treatment G than in treatment D. Finally, although Cyanobacteria (i.e. Zeaxanthin) responded faster to dust addition under future environmental conditions (tanks G), this effect tended to attenuate towards the end of the experiment. In contrast to estimates based on HPLC data, increases in cell abundances did not generally take place until the end of the experiment. While abundances in pico-eukaryotes increased until t96h in treatment D, abundances sharply declined between t72h and t96h for this group in treatment G. The same trend was observed for *Synechococcus* during this experiment, although discrepancies between duplicates in treatment D at sampling time t96h did not allow drawing conclusions on the behavior of this group at the end of the experiment. Both under ambient and future conditions, abundances of nano-eukaryotes declined sharply between t72h and t96h. The decline in HP abundances appeared even earlier during the experiment with moderate maximum relative differences as compared to controls observed at t48h. HP abundances declined very sharply between t48h and t96h in treatment G, reaching control levels, while this decline was less sharp under ambient environmental levels. Finally, HNF dynamics during this experiment was hard to evaluate with no clear effects of dust addition or pH/temperature conditions and with a large increase in abundances in only one duplicate of treatment G (t24h) followed by a gradual decrease.

Abundances of meso-zooplankton at the end of the experiments showed relatively similar values at stations TYR and ION while much higher levels were observed at station FAST (Fig. 9). As a consequence of large variability between duplicates at stations TYR and ION, no clear effects of treatments were detected. At station FAST, although the sample size was too low to statistically test for differences, higher total abundances of meso-zooplankton species were observed in the dust-amended tanks with no differences between ambient and future conditions of temperature and pH. However, differences in abundance were visible between these two

522 treatments for specific groups, with respectively higher abundance of Harosa and lower

523 abundance of Crustacea (other than copepods) and Mollusca in warmed and acidified tanks.

4. Discussion

4.1. Initial conditions

Over the transect, the mixed layer occupied the first 20 m. It was shallower at TYR as compared to ION and FAST (mixed layer depth, MLD of ~ 10 vs ~15 m, respectively) at the time of the sampling (Van Wambeke et al., 2020a). Such shallow MLD is well representative of stratified conditions encountered in the western Mediterranean basin in late spring/early summer (D'Ortenzio et al., 2005). Overall, the three experiments were conducted with surface seawater collected during oligotrophic conditions typical of the open Mediterranean Sea at this period of the year (late spring). Although direct measurements of NO_x and DIP concentrations using nanomolar techniques (as performed in our study) are scarce in the Mediterranean Sea, the low levels measured during the cruise are in agreement with DIP values reported for the three studied basins (Djaoudi et al., 2018) and with NO_x and DIP concentrations measured in coastal waters of Corsica in late spring/early summer (Louis et al., 2017b; Pulido-Villena et al., 2014; Ridame et al., 2014). Furthermore, at all three stations, NO_x:DIP molar ratios in the tested surface waters were well below the Redfield ratio (16:1) and are consistent with ratios found in these previously cited studies. Both low NO_x:DIP ratio and low nutrient concentrations suggest that communities found at the three stations experienced N and P co-limitation at the start of the experiments, as previously shown by Tanaka et al. (2011). A side nutrient enrichment experiment confirmed that, at the three sites, heterotrophic bacteria were mainly N-P co-limited (Van Wambeke et al., 2020b). In contrast to N and P, initial concentrations of dissolved Fe in the sampled seawater, ranging from 1.5 nmol L^{-1} at TYR to 2.5 nmol L^{-1} at ION (Roy-Barman et al., 2020), were unlikely limiting for biological activity as previously shown in the Mediterranean Sea under stratified conditions (Bonnet et al., 2005; Ridame et al., 2014).

Low total chlorophyll *a* concentrations in the tested waters were representative of surface concentrations reported for the Western and Central Mediterranean Sea in late spring/early summer, both from remote sensing images (Bosc et al., 2004), and from *in situ* measurements provided in a database from Manca et al. (2004). While large species (i.e. diatoms, dinoflagellates) represented only ~10% of the total chlorophyll *a* biomass of the tested waters, the composition of the smaller size phytoplankton communities differed substantially. Indeed, communities were clearly dominated by nano-eukaryotes at stations TYR and ION and a larger contribution from pico-eukaryotes and Cyanobacteria was observed at station FAST. Due to their low competitiveness under nutrient limitation, the small contribution of large phytoplankton cells at the start of the experiment is a fingerprint of LNLC areas in general, and of surface Mediterranean waters in late spring and summer (Siokou-Frangou et al., 2010).

As biomass of both heterotrophic nanoflagellates and prokaryotes followed a west to east gradient (FAST > TYR > ION), the ratio of autotrophic vs heterotrophic biomass appeared clearly in favor of the heterotrophic compartment at stations TYR and FAST (ratio of 0.6) while a value above 1 was estimated at ION (ratio of 1.3). This is coherent with the highest net community production (NCP) rates being reported at this station by Gazeau et al. (2021) showing that the initial community at the start of this experiment was very close to metabolic balance (mean ± SE: -0.06 ± 0.09 μmol O_2 L^{-1} d^{-1}). The highest community respiration rates and consequently lowest NCP rates were measured at station TYR (-1.9 μmol O_2 L^{-1} d^{-1}) further suggesting that the autotrophic plankton community was not very active and relying on regenerated nutrients, as shown by the highest level of NH_4^+ measured at the start of this experiment. In contrast, although slightly heterotrophic (Gazeau et al., 2021) and limited by the low amount of nutrients, the community of the tested waters at FAST was the most active as shown by the highest levels of ^{14}C production and heterotrophic prokaryote production (Gazeau et al., 2021) as well as N_2 fixation (Céline Ridame, unpublished results). Altogether, the

heterotrophic signature of the three investigated stations, although closer to metabolic balance at ION, reflected typical biogeochemical conditions in the Mediterranean Sea during late spring to early summer (Regaudie-de-Gioux et al., 2009).

4.2. Critical assessment of the experimental system and methodology

The experimental tanks used in this study have been successfully validated in previous studies designed to investigate the inputs of macro- and micro-nutrients (e.g. NO_x, DIP, DFe) and the export of organic matter, under close-to-abiotic conditions (seawater filtration onto 0.2 µm) following simulated wet dust events using the same analog as used in our study (Bressac and Guieu, 2013; Louis et al., 2017a, 2018). Louis et al. (2017a, 2018) further investigated these impacts under lowered pH conditions, although no control of atmospheric pCO_2 was performed resulting in a rapid increase of pH levels in the acidified filtered seawater due to CO_2 outgassing (from ~7.4 to ~7.7 in six days). Since those above-mentioned studies, in order to avoid this, we improved our experimental system to allow mimicking future conditions by controlling atmospheric pCO_2 in addition to light and temperature (i.e. climate reactors). This allowed to significantly reduce CO_2 outgassing and maintain pH levels close to experimental targets. Still, as illustrated in Fig. 5, the regulation of atmospheric CO_2 was consistently more efficient in tank G2 compared to G1, resulting in a small discrepancy in terms of pH (highest difference of 0.04 pH units between the two G tanks at FAST), possibly due to a potential leak or a longer flushing time above tank G1. Nevertheless, as no systematic differences in terms of biological response were observed between these two tanks, we believe that these small differences in terms of regulated pH had no consequences on the obtained results.

The lids above tanks, equipped with LEDs in order to reproduce sunlight intensity and spectrum, were used for the first time during these experiments. While simulated intensities were

596 close to estimates for the Northwestern Mediterranean Sea at 5 m depth in June (~1100 µmol
597 photons m^{-2} s^{-1}; Bernard Gentili, personal communication, 2017) and fairly consistent between
598 duplicates under control and dust-amended conditions, larger differences were observed between
599 the two warmed and acidified tanks. The reasons of these discrepancies could result from small
600 differences in terms of light intensity regulation between lids, of PAR sensors calibration and/or
601 of different turbidity related to the amount of particles remaining in the tanks. As for pH
602 discussed above, replication in terms of biological response appeared satisfactory for this
603 treatment (except at station TYR; see below), and we believe these technical issues had no
604 significant impacts on our results.

605 Continuous measurements in the tanks showed that temperature was not spatially
606 homogeneous, leading to significant differences among replicates. This was especially the case
607 for warmed tanks (treatment G) for which a maximal average difference over the experimental
608 period of 0.7 °C was observed during the FAST experiment. As for the other controlled
609 parameters discussed above, these discrepancies did not systematically lead to observable
610 differences in the investigated stocks and processes between duplicates (except at TYR, see
611 below).

612 The relatively low number of experimental units that could be installed inside an
613 embarkable clean container restrained our possibility to consider more than two replicates per
614 treatment. Fortunately, as already said, differences between duplicates were, for the vast majority
615 of studied variables and processes, lower than differences between treatments and appear
616 acceptable considering the difficulty to incubate plankton communities for which slight
617 differences in their initial composition can translate into very important differences in dynamics
618 (Eggers et al., 2014). Nevertheless, we have to note that important discrepancies were detected
619 regarding autotrophic stocks and processes (Gazeau et al., 2021) for tanks of the warmed and
620 acidified treatment at station TYR. The reasons behind these differences are not fully understood

but we strongly suspect that heterotrophic nano-flagellates, feeding mainly on prokaryotic picoplankton (Sherr and Sherr, 1994), exerted a strong top-down control on this group in tank G1 in which HNF abundance sharply increased during the experiment. All in all, while the methodology used in this study allowed to successfully evaluate the impacts of dust addition under both present and future environmental conditions at two out of three tested waters, these discrepancies at station TYR prevent us from drawing any strong conclusion on the effect of dust addition on the dynamics of the community under future environmental conditions at that station.

4.3. Impact of dust addition under present environmental conditions

During the three experiments, the observed increases in NO_x and DIP few hours after dust addition under present environmental conditions were rather similar to the enrichment levels obtained during the DUNE experiments at the surface of the mesocosms (~ 50 m^3) after the simulation of a wet dust deposition using the same dust analog and the same simulated flux (Pulido-Villena et al., 2014; Ridame et al., 2014). The intensity of this simulated wet deposition event (i.e. 10 g m^{-2}) represents a high but realistic scenario, as several studies reported even higher short wet deposition events in this area of the Mediterranean Sea (Bonnet and Guieu, 2006; Loÿe-Pilot and Martin, 1996; Ternon et al., 2010). Furthermore, based on previous studies reporting the mixing between dust and polluted air masses during the atmospheric transport of dust particles (e.g. Falkovich et al., 2001; Putaud et al., 2004), we chose to use an evapo-condensed dust analog that mimics the processes taking place in the atmosphere prior to deposition, essentially the adsorption of inorganic and organic soluble species (e.g. sulfate and nitrate; see Guieu et al., 2010a, for further details). The imposed evapo-condensation processes are responsible for the large nitrate releasing capacity of the dust particles used in our study. As a consequence, the addition of new nutrients from dust in our study and during the P and R DUNE

experiments were much higher, especially for NO_x, than those observed by Pitta et al. (2017, and references therein) and Ridame et al. (2014) following the simulation of a dry Saharan dust deposition event. This confirms that wet dust deposition is a more efficient source of bioavailable nutrients compared to dry dust deposition.

Although NO_x and DIP increases after dust addition were rather similar during our three experiments, the subsequent dynamics of these elements and the impacts on plankton community composition and functioning were drastically different. While NO_x levels decreased moderately over the course of our experiments due to biological uptake, more abrupt decreases were observed for DIP released by dust, reaching values close to the ones observed in the controls, except at station FAST where concentrations were still above ambient levels at the end of the experiment.

Regarding biological stocks, most experiments reporting on the effect of dust addition in the Mediterranean Sea showed significant increases in chlorophyll *a* concentrations (mean ~90% increase; Guieu and Ridame, 2020). Interestingly, no stimulation of autotrophic biomass and primary production rates (Gazeau et al., 2021) was observed in dust-amended tanks under present conditions at station TYR. To the best of our knowledge, this is the first experimental evidence of a complete absence of response from an autotrophic community following dust wet deposition. The absence of response from autotrophic stocks could be due to a tight top-down control from grazers hiding potential responses from the autotrophic community (Lekunberri et al., 2010; Marañón et al., 2010) and/or a competition for nutritive resources with heterotrophic prokaryotes (Marañón et al., 2010). Regarding the first hypothesis, Feliú et al. (2020) have shown that the mesozooplankton assemblage at TYR was clearly impacted by a dust event that took place nine days before sampling at that station as evidenced from particulate inventory of lithogenic proxies (Al, Fe) in the water column (Bressac et al., in preparation). This dust deposition likely stimulated phytoplankton growth and consequently increased the abundance of

herbivorous grazers (copepods) and attracted carnivorous species. With respect to the second hypothesis, it is well known that not only phytoplankton but also heterotrophic bacteria are limited by inorganic nutrients, mainly DIP, in oligotrophic systems (Obernosterer et al., 2003; Van Wambeke et al., 2001). Indeed, many recent studies have shown significant increase in heterotrophic bacterial abundance, respiration and/or production following dust deposition (and nutrient enrichment) in these areas (Lekunberri et al., 2010; Pitta et al., 2017; Pulido-Villena et al., 2008; Romero et al., 2011). Most of the time, heterotrophic processes appear to be more stimulated by dust pulses compared to autotrophic processes with increasing degree of oligotrophy, the dominant response being modulated by the competition for nutrients between phytoplankton and bacteria (Marañón et al., 2010). This is clearly what was observed at this station, with heterotrophic prokaryotes reacting quickly and strongly to nutrient addition both in terms of abundances and production rates (Gazeau et al., 2021). These two aforementioned hypotheses are not mutually exclusive, and the quick response of heterotrophic prokaryotes to dust addition is coherent with the strongest net heterotrophy of the tested waters at this station (see 4.1). The strong stimulation of heterotrophic prokaryotes and the absence of detectable effects on the autotrophic compartment drove the community towards an even stronger net heterotrophic state as illustrated by the decrease in the autotrophic to heterotrophic biomass ratio following dust addition (data not shown). This was further shown by increases in community respiration and decreases in net community production rates in dust-amended as compared to control tanks (Gazeau et al., 2021) and suggest that dust addition to surface waters strongly dominated by heterotrophs leads to a reduction of the capacity of these waters to export organic matter and sequester atmospheric CO_2.

In contrast to what was observed at TYR, fertilization of primary producers was observed at stations ION and FAST under present conditions with overall relative changes much higher than from previous studies compiled by Guieu and Ridame (2020). The largest increase in chlorophyll

695 *a* concentrations at station FAST is coherent with the largest NO_x decrease observed in our
696 study, which occurred at this station. Interestingly, following dust addition at this station,
697 autotrophic production did not lead to DIP exhaustion throughout the experiment as DIP
698 concentrations were still above ambient conditions at the end of the experiment. Maximal
699 primary production rates (^{14}C-incorporation) at this station at the end of the experiment suggest a
700 strong DIP recycling and the dominance of regenerated production towards the end of the
701 experiment (Gazeau et al., 2021). Although, in some cases, *Synechococcus* appeared stimulated
702 by dust addition (Herut et al., 2005; Lagaria et al., 2017; Paytan et al., 2009), Guieu et al.
703 (2014b) showed that, based on the analysis of several aerosols addition studies, this group had
704 generally weak responses to aerosol addition in contrast to nano- and micro-phytoplankton,
705 suggesting that aerosol deposition may lead to an increase in larger size class phytoplankton.
706 Yet, at stations ION and FAST, the increase in *Synechococcus* abundance in dust-amended tanks
707 was the highest relative to those of pico- and nano-eukaryotes. This was especially true at station
708 ION where no clear response to nutrient enrichment was observed for nano-eukaryotes
709 throughout the experiment. However, it must be stressed that our experiments were performed
710 over a relatively short period (3 to 4 days), and the sharp increase in Fucoxanthin paralleled by a
711 decrease in silicates, at the end of the experiment at station FAST where DIP limitation was not
712 yet apparent, suggests a delayed response of diatoms as compared to smaller groups (i.e.
713 autotrophic prokaryotes, pico- and nano-eukaryotes). Although this was not observed based on
714 pigment analyses, the sharp decline in nano-eukaryote abundances in dust-amended tanks at the
715 end of the FAST experiment, further suggests that this group, reacting quickly to nutrient
716 enrichment was progressively grazed and/or outcompeted by larger phytoplankton species.

717 In contrast to what was observed at TYR, at station FAST, the competition for nutrients
718 between autotrophs and heterotrophs was clearly in favor of autotrophs with a clear increase in
719 the ratio between autotrophic and heterotrophic biomass reaching values of up to 4 (data not

720 shown). While, as discussed above, all groups of primary producers benefited from nutrient
721 enrichment at this station, the increases in heterotrophic prokaryote abundances were rather
722 limited following dust deposition, leading to an increase of net community production rates
723 throughout this experiment to reach positive levels while control tanks remained below
724 metabolic balance (Gazeau et al., 2021). At station ION, the situation was somewhat
725 intermediate with a similar enhancement of both autotrophic and heterotrophic stocks and no
726 clear changes in the ratio between autotrophic and heterotrophic biomass (data not shown),
727 although the system appeared in favor of net autotrophy at the end of the experiment in dust -
728 amended tanks under present environmental conditions (Gazeau et al., 2021).

729 Transfer of newly produced organic matter to higher trophic levels in the different
730 treatments was evaluated through the quantification of meso-zooplankton abundance at the end
731 of each experiment. Although we are fully aware that such an approach is certainly criticizable
732 considering the low incubation times (3 to 4 days), it may still be representative of lowered
733 mortality or faster growth. Altogether it does not appear as a surprise that an increase in meso-
734 zooplankton abundances was only detected at station FAST where the strongest enhancement of
735 primary production was observed. Such an increase in meso-zooplankton abundance in the dust-
736 amended as compared to control treatment was observed during land-based mesocosm
737 experiments in the Eastern Mediterranean Sea (Pitta et al., 2017).

738 Finally, although no clear effects of dust deposition under present conditions were
739 detectable on autotrophic prokaryotes at station TYR, the strongest increase in N_2 fixation rates
740 was recorded at this station (Céline Ridame, unpublished results). However, the potential impact
741 of this process on NO_x concentration is highly negligible compared to the very large stock of
742 NO_x present in the dust-amended tanks, as less than 1 nmol L^{-1} d^{-1} of NO_x can be produced by
743 this process (Céline Ridame, unpublished results).

4.4. Impact of dust addition under future environmental conditions

Very few past studies have investigated the release and fate of nutrients from atmospheric particles under climate conditions as expected for the end of the century, and, to the best of our knowledge, our study represents the first attempt to test for the combined effect of ocean warming and acidification on these processes. Louis et al. (2018) have already shown from an experiment performed under close-to-abiotic conditions (seawater filtration onto 0.2 μm) that even an extreme ocean acidification scenario (~ -0.6 pH units) does not impact the bioavailability of macro- and micro-nutrients (NO_x, DIP and DFe) from dust addition for surface phytoplankton communities in the oligotrophic Northwestern Mediterranean Sea, using the same dust analog and simulated flux as used during our experiments. Similar results were presented by Mélançon et al. (2016) regarding the release of DFe from dust in high-nutrient low-chlorophyll (HNLC) waters of the Northeastern Pacific, following a mild ocean acidification scenario of -0.2 pH units. As no differences were observed for NO_x and DIP concentrations within few hours following dust addition under present and future environmental conditions, our results agree with these previous findings and further highlights the absence of direct effect of ocean warming (+3 °C) on the release of nutrients from atmospheric particles.

In contrast, following these similar nutrient releases, different nutrient consumption dynamics were observed between ambient and warmed/acidified tanks. These differences were substantially dependent on the considered nutrient and investigated station. Regarding NO_x, no impacts of warming and acidification could be observed at stations TYR and ION due to low net decreasing rates compared to the large increase following dust addition. In contrast, at the most productive station FAST, as a consequence of strongly enhanced biological stocks (see

767 thereafter) and metabolic rates (Gazeau et al., 2021). larger NO_x consumption rates were shown
768 under future environmental conditions.

769 The differences in DIP dynamics between the two dust-amended treatments were more
770 complex to interpret depending on the investigated station. A clear feature of our experiments is
771 that, in contrast to present day pH and temperature conditions, all the stock of DIP released from
772 dust was consumed at the end of the three experiments under future conditions, suggesting a
773 much faster consumption by autotrophs and heterotrophic prokaryotes. That being said, the rate
774 of decrease under future environmental conditions differed depending on the station. While DIP
775 dynamics were quite similar between tanks maintained under present and future environmental
776 conditions at ION, warming and acidification induced a faster decrease of DIP at TYR and
777 FAST, with a full consumption of the released DIP within 24 h. An interesting outcome at station
778 TYR was that, despite the important discrepancies observed for autotrophic stocks and metabolic
779 rates between the duplicates G1 and G2 (see section 4.2), a very similar dynamics was observed
780 for DIP concentrations in these tanks. As heterotrophic prokaryote biomass and production rates
781 (Gazeau et al., 2021) did not differ between these duplicate tanks, this further highlights the clear
782 dominance of heterotrophic processes at this station, a dominance which was exacerbated by dust
783 addition under future environmental conditions, leading to an even stronger heterotrophic state at
784 the end of this experiment (Gazeau et al., 2021).

785 At station ION, large impacts of warming and acidification have been observed,
786 especially for primary producers, as shown by almost doubled chlorophyll *a* concentrations as
787 compared to dust amended tanks (D). At this station, all autotrophic groups benefited from ocean
788 acidification and warming. *Synechococcus* and to a lesser extent pico-eukaryotes appeared as the
789 most impacted ones. Yet these differences of sensitivity among autotrophs did not lead to
790 detectable changes in the composition of the autotrophic assemblage as compared to ambient
791 conditions, with still a large dominance of nano-eukaryote carbon biomass at the end of this

792 experiment (62% in treatment G vs. 64% in treatment D). Interestingly, although the ratio
793 between autotrophic and heterotrophic biomass appeared impacted positively under future
794 environmental conditions, reaching values of up to 2 at the end of this experiment (data not
795 shown), warming and acidification led to a decrease in net community production (Gazeau et al.,
796 2021) suggesting that in the coming decades the capacity of surface seawater to sequester
797 anthropogenic CO_2 will be lowered.

798 Similarly, at FAST, all phytoplankton groups were impacted positively by warming and
799 acidification with the strongest changes detected for *Synechococcus* as compared to present
800 environmental conditions. However, in contrast to station ION, all groups reached maximal
801 abundances (and carbon biomass) after 3 days of incubations, thereafter drastically decreasing
802 most likely as a consequence of DIP limitation (see above). It must be stressed that this pattern
803 could not be observed through pigment dynamics as no sampling was performed for these
804 analyses after 3 days of incubation. Also, in contrast to station ION, the abundance of
805 heterotrophic prokaryotes in the warmer and acidified treatment reached a maximum after 2 days
806 of incubations and then strongly decreased to reach levels observed in the control treatment. This
807 suggests that the heterotrophic compartment was the first to suffer from DIP limitation and
808 further highlights the dominance of the autotrophic compartment in terms of nutrient
809 consumption at this station. As observed at station ION, although the ratio between autotrophic
810 and heterotrophic biomass increased under future environmental conditions, Gazeau et al. (2021)
811 reported on a decrease in net community production rates in this treatment as compared to
812 ambient environmental conditions, suggesting that, in the future, nutrient release from dust will
813 lead to a lesser sequestration capacity of surface waters for atmospheric CO_2.

814 These positive effects of warming and acidification on the abundance of phytoplankton cells,
815 especially for small species, as observed at ION and FAST are in line with previously published
816 studies. Indeed, although very contrasted results have been shown on the effect of ocean

817 acidification on small autotrophic species (e.g. Dutkiewicz et al., 2015), there is increasing
818 evidence that small phytoplankton species will be favored in a warmer ocean (e.g. Chen et al.,
819 2014; Daufresne et al., 2009; Morán et al., 2010). As mentioned earlier, our experimental
820 protocol was not conceived to discriminate temperature from pH effects, however results concur
821 with those of Maugendre et al. (2015) which further suggested temperature over elevated CO_2 as
822 the main driver of increased picophytoplankton abundance in the Mediterranean Sea.

823 These enhanced fertilizing effects on primary producers at ION and FAST, under future
824 as compared to present environmental conditions, did not seem to reach higher trophic levels as
825 no clear differences in meso-zooplankton abundances were observed between ambient and
826 warmed/acidified tanks at the end of the experiments. We fully acknowledge that the duration of
827 our experiments was certainly too short to carefully assess the proportion of newly formed
828 organic matter consumed by meso-zooplankton species and its effect on their abundances, yet
829 group-specific variations were observed. Similarly, Gazeau et al. (2021) did not observe an
830 additional impact of future environmental conditions on the export of organic matter after dust
831 addition.

5. Conclusion

These experiments conducted during the PEACETIME cruise represent the first attempt to investigate the impacts of atmospheric deposition on surface plankton communities both under present and future environmental conditions. Despite few experimental issues that are discussed, the three experiments provided new insights on these potential impacts in the open Mediterranean Sea. Interestingly, the effect of dust deposition was highly different between the three investigated stations in the Tyrrhenian Sea, Ionian Sea and in the Algerian basin. As the initial conditions in the sampled surface seawater at the three stations were very similar in terms of nutrient availability and chlorophyll content, these differences rather seem to be a consequence of the initial metabolic states of the community (autotrophy vs. heterotrophy). In all three cases, nutrient addition from dust deposition did not strongly modify but rather exacerbated this initial state. Relative changes in main parameters presented in this manuscript and processes presented in Gazeau et al. (2021) as a consequence of dust addition under present and future environmental conditions are shown in Fig. 10, and compared to the compilation of published data for the Mediterranean Sea from Guieu and Ridame (2020). At station TYR, under conditions of a clear dominance of heterotrophs on the use of resources and potentially a higher top-down control from grazers, dust addition drove the community into an even more heterotrophic state with no detectable effect on primary producers. At station ION, where the community was initially closer to metabolic balance, both heterotrophic and autotrophic compartments benefited from dust derived nutrients. At FAST, the most active station in terms of autotrophic production, addition of nutrients boosted both compartments but heterotrophic prokaryotes became quickly P-limited and overall larger effects were observed for phytoplankton. Ocean acidification and warming did not have any detectable impact on the release of nutrients from atmospheric particles. Furthermore, these external drivers did not

856 drastically modify the composition of the autotrophic assemblage with all groups benefiting from
857 warmer and acidified conditions. However, although for two out of the three stations
858 investigated, larger increases were observed for autotrophic as compared to heterotrophic stocks
859 under future environmental conditions, a stronger impact of warming and acidification on
860 mineralization processes (Gazeau et al., 2021) suggests that, in the future, the plankton
861 communities of Mediterranean surface waters will have a decreased capacity to sequester
862 atmospheric CO_2 following the deposition of atmospheric particles.

Data availability

All data and metadata will be made available at the French INSU/CNRS LEFE CYBER database (scientific coordinator: Hervé Claustre; data manager, webmaster: Catherine Schmechtig).

INSU/CNRS LEFE CYBER (2020)

Author contributions

FG and CG designed and supervised the study. FG, CG, CR and KD sampled seawater from the experimental tanks during the experiments. JMG and GDL participated in the technical preparation of the experimental system and all authors participated in sample analyses. FG, CR and CG wrote the paper with contributions from all authors.

Financial support

This study is a contribution to the PEACETIME project (http://peacetime-project.org), a joint initiative of the MERMEX and ChArMEx components supported by CNRS-INSU, IFREMER, CEA, and Météo-France as part of the programme MISTRALS coordinated by INSU. PEACETIME is a contribution to SOLAS and IMBER international programme. The project was endorsed as a process study by GEOTRACES. PEACETIME cruise (https://doi.org/10.17600/17000300). The project leading to this publication has also received funding from the European FEDER Fund under project 1166-39417.

Acknowledgments

The authors thank the captain and the crew of the RV Pourquoi Pas ? for their professionalism and their work at sea. We thank Julia Uitz, Céline Dimier and the SAPIGH HPLC analytical service at Institut de la Mer de Villefranche (IMEV) for sampling and analysis of phytoplankton pigments, John Dolan for microscopic countings as well as Lynne Macarez and the PIQv-

885 platform of EMBRC-France, a national Research Infrastructure supported by ANR, under the
886 reference ANR-10-INSB-02, for mesozooplankton analyses.

References

Aminot, A. and Kérouel, R.: Dosage automatique des nutriments dans les eaux marines : méthodes en flux continu, Editions Ifremer, méthodes d'analyse en milieu marin., 2007.

Behrenfeld, M. J., O'Malley, R. T., Siegel, D. A., McClain, C. R., Sarmiento, J. L., Feldman, G. C., Milligan, A. J., Falkowski, P. G., Letelier, R. M. and Boss, E. S.: Climate-driven trends in contemporary ocean productivity, Nature, 444(7120), 752–755, 2006.

Bergametti, Gi., Dutot, A.-L., Buat-Ménard, P., Losno, R. and Remoudaki, E.: Seasonal variability of the elemental composition of atmospheric aerosol particles over the Northwestern Mediterranean, Tellus B: Chemical and Physical Meteorology, 41(3), 353–361, https://doi.org/10.3402/tellusb.v41i3.15092, 1989.

Bonnet, S. and Guieu, C.: Atmospheric forcing on the annual iron cycle in the western Mediterranean Sea: A 1-year survey, Journal of Geophysical Research: Oceans, 111(C9), https://doi.org/10.1029/2005JC003213, 2006.

Bonnet, S., Guieu, C., Chiaverini, J., Ras, J. and Stock, A.: Effect of atmospheric nutrients on the autotrophic communities in a low nutrient, low chlorophyll system, Limnology and Oceanography, 50(6), 1810–1819, https://doi.org/10.4319/lo.2005.50.6.1810, 2005.

Børsheim, K. Y. and Bratbak, G.: Cell volume to cell carbon conversion factors for a bacterivorous Monas sp. enriched from seawater, Marine Ecology Progress Series, 36(2), 171–175, 1987.

Bosc, E., Bricaud, A. and Antoine, D.: Seasonal and interannual variability in algal biomass and primary production in the Mediterranean Sea, as derived from 4 years of SeaWiFS observations, Global Biogeochemical Cycles, 18(1), https://doi.org/10.1029/2003GB002034, 2004.

Bressac, M. and Guieu, C.: Post-depositional processes: What really happens to new atmospheric iron in the ocean's surface?, Global Biogeochemical Cycles, 27(3), 859–870, https://doi.org/10.1002/gbc.20076, 2013.

913 Bressac, M., Wagener, T., Tovar-Sanchez, A., Ridame, C., Albani, S., Fu, F., Desboeufs, K. and
914 Guieu, C.: Residence time of dissolved and particulate trace elements in the surface
915 Mediterranean Sea (Peacetime cruise), Biogeosciences, in preparation.
916 Bressac, M., Guieu, C., Doxaran, D., Bourrin, F., Desboeufs, K., Leblond, N. and Ridame, C.:
917 Quantification of the lithogenic carbon pump following a simulated dust-deposition event
918 in large mesocosms, Biogeosciences, 11(4), 1007–1020, https://doi.org/10.5194/bg-11-
919 1007-2014, 2014.
920 Chen, B., Liu, H., Huang, B. and Wang, J.: Temperature effects on the growth rate of marine
921 picoplankton, Marine Ecology Progress Series, 505, 37–47,
922 https://doi.org/10.3354/meps10773, 2014.
923 Christaki, U., Courties, C., Massana, R., Catala, P., Lebaron, P., Gasol, J. M. and Zubkov, M. V.:
924 Optimized routine flow cytometric enumeration of heterotrophic flagellates using SYBR
925 Green I, Limnology and Oceanography: Methods, 9(8), 329–339,
926 https://doi.org/10.4319/lom.2011.9.329, 2011.
927 Daufresne, M., Lengfellner, K. and Sommer, U.: Global warming benefits the small in aquatic
928 ecosystems, PNAS, 106(31), 12788–12793, https://doi.org/10.1073/pnas.0902080106,
929 2009.
930 Desboeufs, K., Leblond, N., Wagener, T., Bon Nguyen, E. and Guieu, C.: Chemical fate and
931 settling of mineral dust in surface seawater after atmospheric deposition observed from
932 dust seeding experiments in large mesocosms, Biogeosciences, 11(19), 5581–5594,
933 https://doi.org/10.5194/bg-11-5581-2014, 2014.
934 Desboeufs, K., Bon Nguyen, E., Chevaillier, S., Triquet, S. and Dulac, F.: Fluxes and sources of
935 nutrient and trace metal atmospheric deposition in the Northwestern Mediterranean,
936 Atmospheric Chemistry and Physics, 18(19), 14477–14492, https://doi.org/10.5194/acp-
937 18-14477-2018, 2018.

938 Dickson, A. G., Sabine, C. L. and Christian, J. R.: Guide to best practices for ocean CO2
939 measurements, PICES, Sydney., 2007.
940 Dinasquet, J., Bigeard, E., Gazeau, F., Marañón, E., Ridame, C., Van Wambeke, F.,
941 Obernosterer, I. and Baudoux, A.-C.: Impact of dust enrichment on the microbial food web
942 under present and future conditions of pH and temperature, Biogeosciences Discussions,
943 2021.
944 Djaoudi, K., Van Wambeke, F., Coppola, L., D'Ortenzio, F., Helias-Nunige, S., Raimbault, P.,
945 Taillandier, V., Testor, P., Wagener, T. and Pulido-Villena, E.: Sensitive Determination of
946 the Dissolved Phosphate Pool for an Improved Resolution of Its Vertical Variability in the
947 Surface Layer: New Views in the P-Depleted Mediterranean Sea, Front. Mar. Sci., 5,
948 https://doi.org/10.3389/fmars.2018.00234, 2018.
949 D'Ortenzio, F., Iudicone, D., Montegut, C. de B., Testor, P., Antoine, D., Marullo, S., Santoleri,
950 R. and Madec, G.: Seasonal variability of the mixed layer depth in the Mediterranean Sea
951 as derived from in situ profiles, Geophysical Research Letters, 32(12),
952 https://doi.org/10.1029/2005GL022463, 2005.
953 Duce, R. A., Liss, P. S., Merrill, J. T., Atlas, E. L., Buat-Menard, P., Hicks, B. B., Miller, J. M.,
954 Prospero, J. M., Arimoto, R., Church, T. M., Ellis, W., Galloway, J. N., Hansen, L.,
955 Jickells, T. D., Knap, A. H., Reinhardt, K. H., Schneider, B., Soudine, A., Tokos, J. J.,
956 Tsunogai, S., Wollast, R. and Zhou, M.: The atmospheric input of trace species to the
957 world ocean, Global Biogeochemical Cycles, 5(3), 193–259,
958 https://doi.org/10.1029/91GB01778, 1991.
959 Dutkiewicz, S., Morris, J. J., Follows, M. J., Scott, J., Levitan, O., Dyhrman, S. T. and Berman-
960 Frank, I.: Impact of ocean acidification on the structure of future phytoplankton
961 communities, Nature Climate change, 5, 1002–1006, https://doi.org/10.1038/nclimate2722,
962 2015.

963 Emerson, S., Quay, P., Karl, D., Winn, C., Tupas, L. and Landry, M.: Experimental
964 determination of the organic carbon flux from open-ocean surface waters, Nature,
965 389(6654), 951–954, https://doi.org/10.1038/40111, 1997.
966 Falkovich, A. H., Ganor, E., Levin, Z., Formenti, P. and Rudich, Y.: Chemical and mineralogical
967 analysis of individual mineral dust particles, Journal of Geophysical Research:
968 Atmospheres, 106(D16), 18029–18036, https://doi.org/10.1029/2000JD900430, 2001.
969 Feliú, G., Pagano, M., Hidalgo, P. and Carlotti, F.: Structure and function of epipelagic
970 mesozooplankton and their response to dust deposition events during the spring
971 PEACETIME cruise in the Mediterranean Sea, Biogeosciences, 17, 5417–5441,
972 https://doi.org/10.5194/bg-17-5417-2020, 2020.
973 Gazeau, F., Van Wambeke, F., Marañón, E., Pérez-Lorenzo, M., Alliouane, S., Stolpe, C.,
974 Blasco, T., Leblond, N., Zäncker, B., Engel, A., Marie, B., Dinasquet, J. and Guieu, C.:
975 Impact of dust addition on the metabolism of Mediterranean plankton communities and
976 carbon export under present and future conditions of pH and temperature, Biogeosciences
977 Discussions, 2021.
978 Giovagnetti, V., Brunet, C., Conversano, F., Tramontano, F., Obernosterer, I., Ridame, C. and
979 Guieu, C.: Assessing the role of dust deposition on phytoplankton ecophysiology and
980 succession in a low-nutrient low-chlorophyll ecosystem: a mesocosm experiment in the
981 Mediterranean Sea, Biogeosciences, 10(5), 2973–2991, https://doi.org/10.5194/bg-10-
982 2973-2013, 2013.
983 Gorsky, G., Ohman, M. D., Picheral, M., Gasparini, S., Stemmann, L., Romagnan, J.-B.,
984 Cawood, A., Pesant, S., García-Comas, C. and Prejger, F.: Digital zooplankton image
985 analysis using the ZooScan integrated system, J Plankton Res, 32(3), 285–303,
986 https://doi.org/10.1093/plankt/fbp124, 2010.
987 Guieu, C. and Ridame, C.: Impact of atmospheric deposition on marine chemistry and
988 biogeochemistry, in Atmospheric Chemistry in the Mediterranean Region: Comprehensive

989 Diagnosis and Impacts, edited by F. Dulac, S. Sauvage, and E. Hamonou, Springer, Cham,
990 Switzerland, , 2020.
991 Guieu, C., Dulac, F., Desboeufs, K., Wagener, T., Pulido-Villena, E., Grisoni, J.-M., Louis, F.,
992 Ridame, C., Blain, S., Brunet, C., Bon Nguyen, E., Tran, S., Labiadh, M. and Dominici, J.-
993 M.: Large clean mesocosms and simulated dust deposition: a new methodology to
994 investigate responses of marine oligotrophic ecosystems to atmospheric inputs,
995 Biogeosciences, 7(9), 2765–2784, https://doi.org/10.5194/bg-7-2765-2010, 2010a.
996 Guieu, C., Loye-Pilot, M. D., Benyahya, L. and Dufour, A.: Spatial variability of atmospheric
997 fluxes of metals (Al, Fe, Cd, Zn and Pb) and phosphorus over the whole Mediterranean
998 from a one-year monitoring experiment: Biogeochemical implications, Marine Chemistry,
999 120(1–4), 164–178, https://doi.org/10.1016/j.marchem.2009.02.004, 2010b.
1000 Guieu, C., Ridame, C., Pulido-Villena, E., Bressac, M., Desboeufs, K. and Dulac, F.: Impact of
1001 dust deposition on carbon budget: a tentative assessment from a mesocosm approach,
1002 Biogeosciences, 11(19), 5621–5635, 2014a.
1003 Guieu, C., Aumont, O., Paytan, A., Bopp, L., Law, C. S., Mahowald, N., Achterberg, E. P.,
1004 Marañón, E., Salihoglu, B., Crise, A., Wagener, T., Herut, B., Desboeufs, K., Kanakidou,
1005 M., Olgun, N., Peters, F., Pulido-Villena, E., Tovar-Sanchez, A. and Völker, C.: The
1006 significance of the episodic nature of atmospheric deposition to Low Nutrient Low
1007 Chlorophyll regions, Global Biogeochemical Cycles, 28(11), 1179–1198,
1008 https://doi.org/10.1002/2014GB004852, 2014b.
1009 Guieu, C., D'Ortenzio, F., Dulac, F., Taillandier, V., Doglioli, A., Petrenko, A., Barrillon, S.,
1010 Mallet, M., Nabat, P. and Desboeufs, K.: Process studies at the air-sea interface after
1011 atmospheric deposition in the Mediterranean Sea: objectives and strategy of the
1012 PEACETIME oceanographic campaign (May–June 2017), Biogeosciences, 2020(17),
1013 5563–5585, https://doi.org/10.5194/bg-17-5563-2020, 2020.

1014 Herut, B., Zohary, T., Krom, M. D., Mantoura, R. F. C., Pitta, P., Psarra, S., Rassoulzadegan, F.,
1015 Tanaka, T. and Frede Thingstad, T.: Response of East Mediterranean surface water to
1016 Saharan dust: On-board microcosm experiment and field observations, Deep Sea Research
1017 Part II: Topical Studies in Oceanography, 52(22), 3024–3040,
1018 https://doi.org/10.1016/j.dsr2.2005.09.003, 2005.
1019 Holmes, R. M., Aminot, A., Kérouel, R., Hooker, B. A. and Peterson, B. J.: A simple and precise
1020 method for measuring ammonium in marine and freshwater ecosystems, Can. J. Fish.
1021 Aquat. Sci., 56(10), 1801–1808, https://doi.org/10.1139/f99-128, 1999.
1022 IPCC: Climate Change, The Physical Science Basis., 2013.
1023 IPCC: IPCC Special Report on the Ocean and Cryosphere in a Changing Climate, edited by H.
1024 O. Pörtner, D. C. Roberts, V. Masson-Delmotte, P. Zhai, M. Tignor, E. Poloczanska, K.
1025 Mintenbeck, A. Alegría, M. Nicolai, A. Okem, J. Petzold, B. Rama, and N. M. Weyer.,
1026 2019.
1027 Irwin, A. J. and Oliver, M. J.: Are ocean deserts getting larger?, Geophysical Research Letters,
1028 36, https://doi.org/10.1029/2009gl039883, 2009.
1029 Jickells, T. D., An, Z. S., Andersen, K. K., Baker, A. R., Bergametti, G., Brooks, N., Cao, J. J.,
1030 Boyd, P. W., Duce, R. A., Hunter, K. A., Kawahata, H., Kubilay, N., laRoche, J., Liss, P.
1031 S., Mahowald, N., Prospero, J. M., Ridgwell, A. J., Tegen, I. and Torres, R.: Global Iron
1032 Connections Between Desert Dust, Ocean Biogeochemistry, and Climate, Science,
1033 308(5718), 67–71, https://doi.org/10.1126/science.1105959, 2005.
1034 Kana, T. M. and Glibert, P. M.: Effect of irradiances up to 2000 μE m^{-2} s^{-1} on marine
1035 *Synechococcus* WH7803—I. Growth, pigmentation, and cell composition, Deep Sea
1036 Research Part A. Oceanographic Research Papers, 34(4), 479–495,
1037 https://doi.org/10.1016/0198-0149(87)90001-X, 1987.

1038 Kapsenberg, L., Alliouane, S., Gazeau, F., Mousseau, L. and Gattuso, J.-P.: Coastal ocean
1039 acidification and increasing total alkalinity in the northwestern Mediterranean Sea, Ocean
1040 Science, 13, 411–426, https://doi.org/10.5194/os-13-411-2017, 2017.
1041 Kouvarakis, G., Mihalopoulos, N., Tselepides, A. and Stavrakakis, S.: On the importance of
1042 atmospheric inputs of inorganic nitrogen species on the productivity of the Eastern
1043 Mediterranean Sea, Global Biogeochemical Cycles, 15(4), 805–817,
1044 https://doi.org/10.1029/2001GB001399, 2001.
1045 Lagaria, A., Mandalakis, M., Mara, P., Papageorgiou, N., Pitta, P., Tsiola, A., Kagiorgi, M. and
1046 Psarra, S.: Phytoplankton response to Saharan dust depositions in the Eastern
1047 Mediterranean Sea: A mesocosm study, Front. Mar. Sci., 3,
1048 https://doi.org/10.3389/fmars.2016.00287, 2017.
1049 Law, C. S., Brévière, E., de Leeuw, G., Garçon, V., Guieu, C., Kieber, D. J., Kontradowitz, S.,
1050 Paulmier, A., Quinn, P. K., Saltzman, E. S., Stefels, J. and von Glasow, R.: Evolving
1051 research directions in Surface Ocean - Lower Atmosphere (SOLAS) science, Environ.
1052 Chem., 10(1), 1, https://doi.org/10.1071/EN12159, 2013.
1053 Lee, S. and Fuhrman, J. A.: Relationships between Biovolume and Biomass of Naturally Derived
1054 Marine Bacterioplankton, Appl Environ Microbiol, 53(6), 1298–1303, 1987.
1055 Lekunberri, I., Lefort, T., Romero, E., Vázquez-Domínguez, E., Romera-Castillo, C., Marrasé,
1056 C., Peters, F., Weinbauer, M. and Gasol, J. M.: Effects of a dust deposition event on
1057 coastal marine microbial abundance and activity, bacterial community structure and
1058 ecosystem function, J Plankton Res, 32(4), 381–396,
1059 https://doi.org/10.1093/plankt/fbp137, 2010.
1060 Liu, X., Patsavas, M. C. and Byrne, R. H.: Purification and Characterization of meta-Cresol
1061 Purple for Spectrophotometric Seawater pH Measurements, Environ. Sci. Technol., 45(11),
1062 4862–4868, https://doi.org/10.1021/es200665d, 2011.

1063 Longhurst, A., Sathyendranath, S., Platt, T. and Caverhill, C.: An estimate of global primary
1064 production in the ocean from satellite radiometer data, Journal of Plankton Research, 17(6),
1065 1245–1271, https://doi.org/10.1093/plankt/17.6.1245, 1995.
1066 López-Urrutia, A. and Morán, X. A. G.: Resource limitation of bacterial production distorts the
1067 temperature dependence of oceanic carbon cycling, Ecology, 88(4), 817–822,
1068 https://doi.org/10.1890/06-1641, 2007.
1069 Louis, J., Pedrotti, M. L., Gazeau, F. and Guieu, C.: Experimental evidence of formation of
1070 transparent exopolymer particles (TEP) and POC export provoked by dust addition under
1071 current and high pCO_2 conditions, PLOS ONE, 12(2), e0171980,
1072 https://doi.org/10.1371/journal.pone.0171980, 2017a.
1073 Louis, J., Guieu, C. and Gazeau, F.: Nutrient dynamics under different ocean acidification
1074 scenarios in a low nutrient low chlorophyll system: The Northwestern Mediterranean Sea,
1075 Estuarine, Coastal and Shelf Science, 186, 30–44,
1076 https://doi.org/10.1016/j.ecss.2016.01.015, 2017b.
1077 Louis, J., Gazeau, F. and Guieu, C.: Atmospheric nutrients in seawater under current and high
1078 pCO_2 conditions after Saharan dust deposition: Results from three minicosm experiments,
1079 Progress in Oceanography, 163, 40–49, https://doi.org/10.1016/j.pocean.2017.10.011,
1080 2018.
1081 Loÿe-Pilot, M. D. and Martin, J. M.: Saharan Dust Input to the Western Mediterranean: An
1082 Eleven Years Record in Corsica, in The Impact of Desert Dust Across the Mediterranean,
1083 edited by S. Guerzoni and R. Chester, pp. 191–199, Springer Netherlands, Dordrecht,
1084 https://doi.org/10.1007/978-94-017-3354-0_18, , 1996.
1085 Manca, B., Burca, M., Giorgetti, A., Coatanoan, C., Garcia, M.-J. and Iona, A.: Physical and
1086 biochemical averaged vertical profiles in the Mediterranean regions: an important tool to
1087 trace the climatology of water masses and to validate incoming data from operational

oceanography, Journal of Marine Systems, 48(1), 83–116, https://doi.org/10.1016/j.jmarsys.2003.11.025, 2004.

Marañón, E., Fernández, A., Mouriño-Carballido, B., MartÍnez-GarcÍa, S., Teira, E., Cermeño, P., Chouciño, P., Huete-Ortega, M., Fernández, E., Calvo-DÍaz, A., Morán, X. A. G., Bode, A., Moreno-Ostos, E., Varela, M. M., Patey, M. D. and Achterberg, E. P.: Degree of oligotrophy controls the response of microbial plankton to Saharan dust, Limnology and Oceanography, 55(6), 2339–2352, https://doi.org/10.4319/lo.2010.55.6.2339, 2010.

Marañón, E., Lorenzo, M. P., Cermeño, P. and Mouriño-Carballido, B.: Nutrient limitation suppresses the temperature dependence of phytoplankton metabolic rates, The ISME Journal, 12(7), 1836–1845, https://doi.org/10.1038/s41396-018-0105-1, 2018.

Marie, D., Simon, N., Guillou, L., Partensky, F. and Vaulot, D.: Flow cytometry analysis of marine picoplankton, in living color: protocols in flow cytometry and cell sorting, edited by R. A. Diamond and S. DeMaggio, pp. 421–454, Springer, Berlin, , 2010.

Markaki, Z., Oikonomou, K., Kocak, M., Kouvarakis, G., Chaniotaki, A., Kubilay, N. and Mihalopoulos, N.: Atmospheric deposition of inorganic phosphorus in the Levantine Basin, eastern Mediterranean: Spatial and temporal variability and its role in seawater productivity, Limnology and Oceanography, 48(4), 1557–1568, https://doi.org/10.4319/lo.2003.48.4.1557, 2003.

Maugendre, L., Gattuso, J.-P., Louis, J., de Kluijver, A., Marro, S., Soetaert, K. and Gazeau, F.: Effect of ocean warming and acidification on a plankton community in the NW Mediterranean Sea, ICES Journal of Marine Science, 72(6), 1744–1755, https://doi.org/10.1093/icesjms/fsu161, 2015.

Maugendre, L., Guieu, C., Gattuso, J.-P. and Gazeau, F.: Ocean acidification in the Mediterranean Sea: Pelagic mesocosm experiments. A synthesis, Estuarine, Coastal and Shelf Science, 186, 1–10, https://doi.org/10.1016/j.ecss.2017.01.006, 2017.

Mayot, N., D'Ortenzio, F., Ribera d'Alcalà, M., Lavigne, H. and Claustre, H.: Interannual variability of the Mediterranean trophic regimes from ocean color satellites, Biogeosciences, 13(6), 1901–1917, https://doi.org/10.5194/bg-13-1901-2016, 2016.

Mélançon, J., Levasseur, M., Lizotte, M., Scarratt, M., Tremblay, J.-É., Tortell, P., Yang, G.-P., Shi, G.-Y., Gao, H., Semeniuk, D., Robert, M., Arychuk, M., Johnson, K., Sutherland, N., Davelaar, M., Nemcek, N., Peña, A. and Richardson, W.: Impact of ocean acidification on phytoplankton assemblage, growth, and DMS production following Fe-dust additions in the NE Pacific high-nutrient, low-chlorophyll waters, Biogeosciences, 13(5), 1677–1692, https://doi.org/10.5194/bg-13-1677-2016, 2016.

Moore, C. M., Mills, M. M., Arrigo, K. R., Berman-Frank, I., Bopp, L., Boyd, P. W., Galbraith, E. D., Geider, R. J., Guieu, C., Jaccard, S. L., Jickells, T. D., La Roche, J., Lenton, T. M., Mahowald, N. M., Marañón, E., Marinov, I., Moore, J. K., Nakatsuka, T., Oschlies, A., Saito, M. A., Thingstad, T. F., Tsuda, A. and Ulloa, O.: Processes and patterns of oceanic nutrient limitation, Nature Geoscience, 6(9), 701–710, https://doi.org/10.1038/ngeo1765, 2013.

Morán, X. A. G., López-Urrutia, Á., Calvo-Díaz, A. and Li, W. K. W.: Increasing importance of small phytoplankton in a warmer ocean, Global Change Biology, 16(3), 1137–1144, https://doi.org/10.1111/j.1365-2486.2009.01960.x, 2010.

Neale, P. J., Sobrino, C., Segovia, M., Mercado, J. M., Leon, P., Cortés, M. D., Tuite, P., Picazo, A., Salles, S., Cabrerizo, M. J., Prasil, O., Montecino, V., Reul, A. and Fuentes-Lema, A.: Effect of CO2, nutrients and light on coastal plankton. I. Abiotic conditions and biological responses, Aquatic Biology, 22, 25–41, https://doi.org/10.3354/ab00587, 2014.

Obernosterer, I., Kawasaki, N. and Benner, R.: P-limitation of respiration in the Sargasso Sea and uncoupling of bacteria from P-regeneration in size-fractionation experiments, Aquatic Microbial Ecology, 32(3), 229–237, https://doi.org/10.3354/ame032229, 2003.

1138 Orr, J. C., Epitalon, J.-M., Dickson, A. G. and Gattuso, J.-P.: Routine uncertainty propagation for
1139 the marine carbon dioxide system, Marine Chemistry, 207, 84–107,
1140 https://doi.org/10.1016/j.marchem.2018.10.006, 2018.
1141 Paytan, A., Mackey, K. R. M., Chen, Y., Lima, I. D., Doney, S. C., Mahowald, N., Labiosa, R.
1142 and Post, A. F.: Toxicity of atmospheric aerosols on marine phytoplankton, Proceedings of
1143 the National Academy of Sciences, 106(12), 4601–4605,
1144 https://doi.org/10.1073/pnas.0811486106, 2009.
1145 Pitta, P., Kanakidou, M., Mihalopoulos, N., Christodoulaki, S., Dimitriou, P. D., Frangoulis, C.,
1146 Giannakourou, A., Kagiorgi, M., Lagaria, A., Nikolaou, P., Papageorgiou, N., Psarra, S.,
1147 Santi, I., Tsapakis, M., Tsiola, A., Violaki, K. and Petihakis, G.: Saharan Dust Deposition
1148 Effects on the Microbial Food Web in the Eastern Mediterranean: A Study Based on a
1149 Mesocosm Experiment, Front. Mar. Sci., 4, https://doi.org/10.3389/fmars.2017.00117,
1150 2017.
1151 Polovina, J. J., Howell, E. A. and Abecassis, M.: Ocean's least productive waters are expanding,
1152 Geophysical Research Letters, 35(3), https://doi.org/10.1029/2007gl031745, 2008.
1153 Powley, H. R., Krom, M. D. and Cappellen, P. V.: Understanding the unique biogeochemistry of
1154 the Mediterranean Sea: Insights from a coupled phosphorus and nitrogen model, Global
1155 Biogeochemical Cycles, 31(6), 1010–1031, https://doi.org/10.1002/2017GB005648, 2017.
1156 Pulido-Villena, E., Wagener, T. and Guieu, C.: Bacterial response to dust pulses in the western
1157 Mediterranean: Implications for carbon cycling in the oligotrophic ocean, Global
1158 Biogeochemical Cycles, 22(1), https://doi.org/10.1029/2007gb003091, 2008.
1159 Pulido-Villena, E., Rerolle, V. and Guieu, C.: Transient fertilizing effect of dust in P-deficient
1160 LNLC surface ocean, Geophysical Research Letters, 37,
1161 https://doi.org/10.1029/2009gl041415, 2010.
1162 Pulido-Villena, E., Baudoux, A.-C., Obernosterer, I., Landa, M., Caparros, J., Catala, P.,
1163 Georges, C., Harmand, J. and Guieu, C.: Microbial food web dynamics in response to a

Saharan dust event: results from a mesocosm study in the oligotrophic Mediterranean Sea, Biogeosciences, 11(19), 5607–5619, 2014.

Putaud, J.-P., Dingenen, R. V., Dell'Acqua, A., Raes, F., Matta, E., Decesari, S., Facchini, M. C. and Fuzzi, S.: Size-segregated aerosol mass closure and chemical composition in Monte Cimone (I) during MINATROC, Atmospheric Chemistry and Physics, 4(4), 889–902, https://doi.org/10.5194/acp-4-889-2004, 2004.

Ras, J., Claustre, H. and Uitz, J.: Spatial variability of phytoplankton pigment distributions in the Subtropical South Pacific Ocean: comparison between in situ and predicted data, Biogeosciences, 5(2), 353–369, https://doi.org/10.5194/bg-5-353-2008, 2008.

Regaudie-de-Gioux, A., Vaquer-Sunyer, R. and Duarte, C. M.: Patterns in planktonic metabolism in the Mediterranean Sea, Biogeosciences, 6(12), 3081–3089, https://doi.org/10.5194/bg-6-3081-2009, 2009.

Richon, C., Dutay, J.-C., Dulac, F., Wang, R., Balkanski, Y., Nabat, P., Aumont, O., Desboeufs, K., Laurent, B., Guieu, C., Raimbault, P. and Beuvier, J.: Modeling the impacts of atmospheric deposition of nitrogen and desert dust-derived phosphorus on nutrients and biological budgets of the Mediterranean Sea, Progress in Oceanography, 163, 21–39, https://doi.org/10.1016/j.pocean.2017.04.009, 2018.

Ridame, C. and Guieu, C.: Saharan input of phosphate to the oligotrophic water of the open western Mediterranean Sea, Limnology and Oceanography, 47(3), 856–869, 2002.

Ridame, C., Guieu, C. and L'Helguen, S.: Strong stimulation of N 2 fixation in oligotrophic Mediterranean Sea: results from dust addition in large in situ mesocosms, Biogeosciences, 10(11), 7333–7346, 2013.

Ridame, C., Dekaezemacker, J., Guieu, C., Bonnet, S., L'Helguen, S. and Malien, F.: Contrasted Saharan dust events in LNLC environments: impact on nutrient dynamics and primary production, Biogeosciences (BG), 11(17), 4783–4800, 2014.

Romero, E., Peters, F., Marrasé, C., Guadayol, Ò., Gasol, J. M. and Weinbauer, M. G.: Coastal Mediterranean plankton stimulation dynamics through a dust storm event: An experimental simulation, Estuarine, Coastal and Shelf Science, 93(1), 27–39, https://doi.org/10.1016/j.ecss.2011.03.019, 2011.

Roy-Barman, M., Folio, L., Douville, E., Leblond, N., Gazeau, F., Bressac, M., Wagener, T., Ridame, C., Desboeufs, K. and Guieu, C.: Contrasted release of insoluble elements (Fe, Al, REE, Th, Pa) after dust deposition in seawater: a tank experiment approach, Biogeosciences Discussions, 1–27, https://doi.org/10.5194/bg-2020-247, 2020.

Sala, M. M., Aparicio, F. L., Balagué, V., Boras, J. A., Borrull, E., Cardelús, C., Cros, L., Gomes, A., López-Sanz, A., Malits, A., Martínez, R. A., Mestre, M., Movilla, J., Sarmento, H., Vázquez-Domínguez, E., Vaqué, D., Pinhassi, J., Calbet, A., Calvo, E., Gasol, J. M., Pelejero, C. and Marrasé, C.: Contrasting effects of ocean acidification on the microbial food web under different trophic conditions, ICES Journal of Marine Science, 73(3), 670–679, https://doi.org/10.1093/icesjms/fsv130, 2016.

Sherr, E. B. and Sherr, B. F.: Bacterivory and herbivory: Key roles of phagotrophic protists in pelagic food webs, Microb Ecol, 28(2), 223–235, https://doi.org/10.1007/BF00166812, 1994.

Siokou-Frangou, I., Christaki, U., Mazzocchi, M. G., Montresor, M., Ribera d'Alcalá, M., Vaqué, D. and Zingone, A.: Plankton in the open Mediterranean Sea: a review, Biogeosciences, 7(5), 1543–1586, https://doi.org/10.5194/bg-7-1543-2010, 2010.

Tanaka, T., Thingstad, T. F., Christaki, U., Colombet, J., Cornet-Barthaux, V., Courties, C., Grattepanche, J.-D., Lagaria, A., Nedoma, J., Oriol, L., Psarra, S., Pujo-Pay, M. and Wambeke, F. V.: Lack of P-limitation of phytoplankton and heterotrophic prokaryotes in surface waters of three anticyclonic eddies in the stratified Mediterranean Sea, Biogeosciences, 8(2), 525–538, https://doi.org/10.5194/bg-8-525-2011, 2011.

1214 Ternon, E., Guieu, C., Loÿe-Pilot, M.-D., Leblond, N., Bosc, E., Gasser, B., Miquel, J.-C. and
1215 Martín, J.: The impact of Saharan dust on the particulate export in the water column of the
1216 North Western Mediterranean Sea, Biogeosciences, 7(3), 809–826,
1217 https://doi.org/10.5194/bg-7-809-2010, 2010.
1218 The Mermex group: Marine ecosystems' responses to climatic and anthropogenic forcings in the
1219 Mediterranean, Progress in Oceanography, 91(2), 97–166,
1220 https://doi.org/10.1016/j.pocean.2011.02.003, 2011.
1221 Theodosi, C., Markaki, Z., Tselepides, A. and Mihalopoulos, N.: The significance of atmospheric
1222 inputs of soluble and particulate major and trace metals to the eastern Mediterranean
1223 seawater, Marine Chemistry, 120(1), 154–163,
1224 https://doi.org/10.1016/j.marchem.2010.02.003, 2010.
1225 Van Wambeke, F., Goutx, M., Striby, L., Sempéré, R. and Vidussi, F.: Bacterial dynamics
1226 during the transition from spring bloom to oligotrophy in the northwestern Mediterranean
1227 Sea: relationships with particulate detritus and dissolved organic matter, Marine Ecology
1228 Progress Series, 212, 89–105, 2001.
1229 Van Wambeke, F., Taillandier, V., Deboeufs, K., Pulido-Villena, E., Dinasquet, J., Engel, A.,
1230 Marañón, E., Ridame, C. and Guieu, C.: Influence of atmospheric deposition on
1231 biogeochemical cycles in an oligotrophic ocean system, Biogeosciences Discussions, 1–51,
1232 https://doi.org/10.5194/bg-2020-411, 2020a.
1233 Van Wambeke, F., Pulido, E., Dinasquet, J., Djaoudi, K., Engel, A., Garel, M., Guasco, S.,
1234 Nunige, S., Taillandier, V., Zäncker, B. and Tamburini, C.: Spatial patterns of biphasic
1235 ectoenzymatic kinetics related to biogeochemical properties in the Mediterranean Sea,
1236 Biogeosciences Discussions, 1–38, https://doi.org/10.5194/bg-2020-253, 2020b.
1237 Verity, P. G., Robertson, C. Y., Tronzo, C. R., Andrews, M. G., Nelson, J. R. and Sieracki, M.
1238 E.: Relationships between cell volume and the carbon and nitrogen content of marine

photosynthetic nanoplankton, Limnology and Oceanography, 37(7), 1434–1446, https://doi.org/10.4319/lo.1992.37.7.1434, 1992.

Vidussi, F., Claustre, H., Manca, B. B., Luchetta, A. and Marty, J.-C.: Phytoplankton pigment distribution in relation to upper thermocline circulation in the eastern Mediterranean Sea during winter, Journal of Geophysical Research: Oceans, 106(C9), 19939–19956, https://doi.org/10.1029/1999JC000308, 2001.

Table 1. List of parameters and processes investigated during the three experiments at stations TYR, ION and FAST. Related manuscripts are indicated. pH_T: pH on the total scale, A_T: total alkalinity, ^{13}C-C_T: ^{13}C signature of dissolved inorganic carbon, NO_x: nitrate + nitrite, DIP: dissolved inorganic phosphorus, $Si(OH)_4$: silicate, DFe: dissolved iron, DAl: dissolved aluminium, Th-REE-Pa: Thorium (^{230}Th and ^{232}Th), Rare Earth elements and Protactinium (^{231}Pa), POC: particulate organic carbon, DOC: dissolved organic carbon, ^{13}C-DOC: ^{13}C signature of dissolved organic carbon, TEP: transparent exopolymer particles, NCP/CR: net community production and community respiration (oxygen based), ^{14}C-PP: primary production based on ^{14}C incorporation.

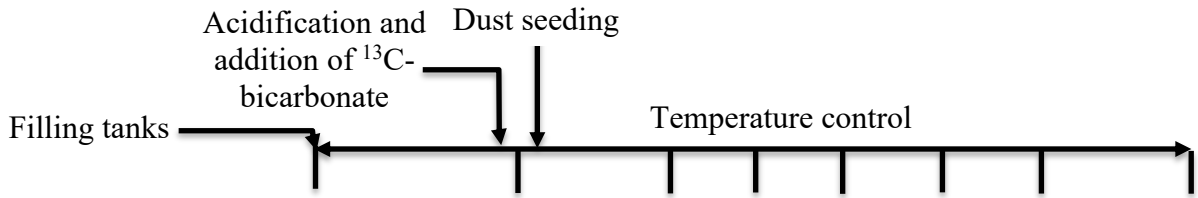

		Related manuscript
Temperature	Continuous	This manuscript
Irradiance	Continuous	This manuscript

Carbonate chemistry

pH_T		This manuscript
A_T		This manuscript
$\delta^{13}C$-C_T		Gazeau et al. (2021)

Macro-nutrients

NO_x		This manuscript
DIP		This manuscript
$Si(OH)_4$		This manuscript

Micro-nutrients

DFe		Roy-Barman et al. (2020)
DAl		Roy-Barman et al. (2020)
Th-REE-Pa		Roy-Barman et al. (2020)

Biological stocks

Pigments		This manuscript
Flow cytometry		This manuscript

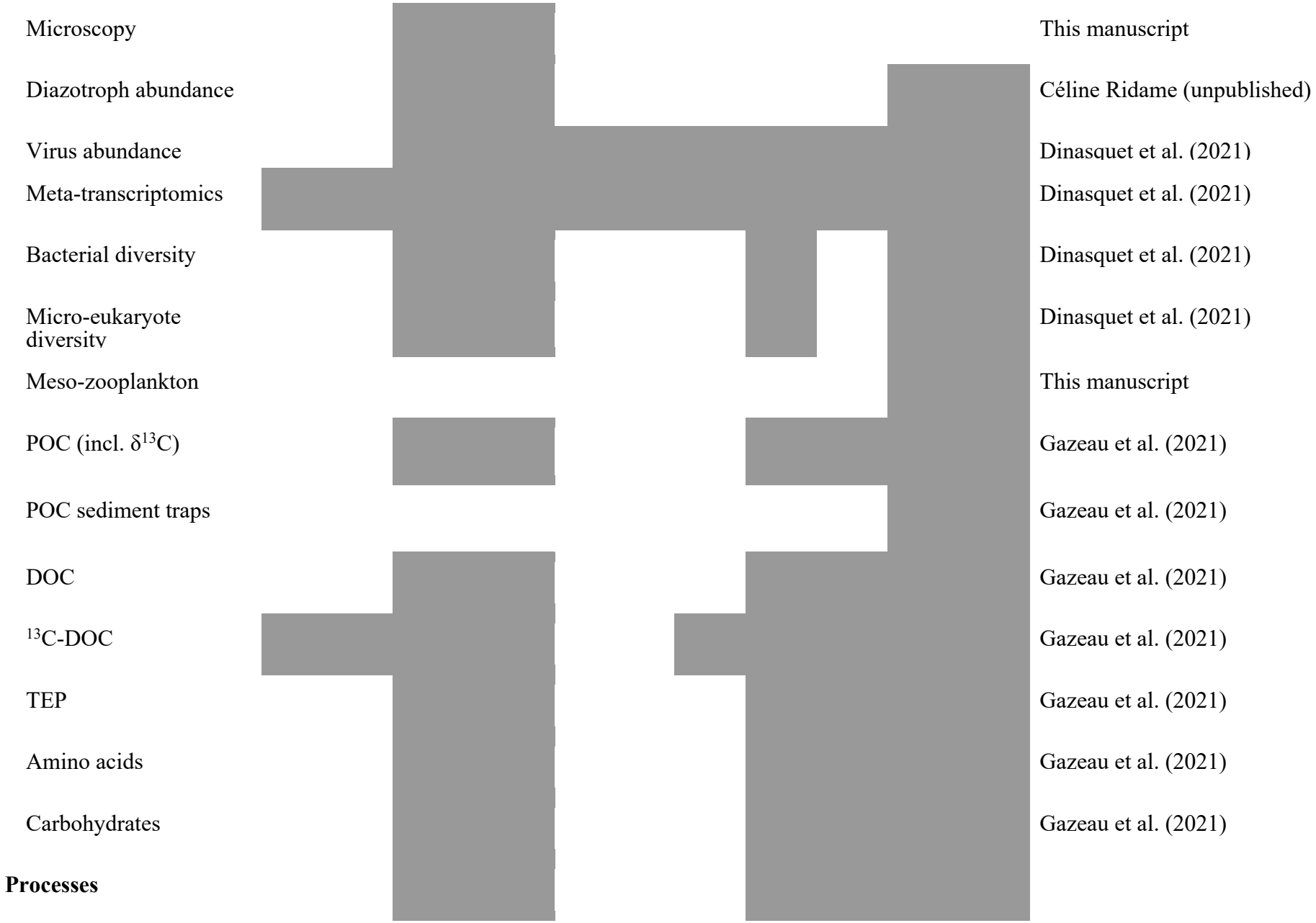
Microscopy
This manuscript
Diazotroph abundance
Céline Ridame (unpublished)
Virus abundance
Dinasquet et al. (2021)
Meta-transcriptomics
Dinasquet et al. (2021)
Bacterial diversity
Dinasquet et al. (2021)
Micro-eukaryote diversity
Dinasquet et al. (2021)
Meso-zooplankton
This manuscript
POC (incl. δ13C)
Gazeau et al. (2021)
POC sediment traps
Gazeau et al. (2021)
DOC
Gazeau et al. (2021)
13C-DOC
Gazeau et al. (2021)
TEP
Gazeau et al. (2021)
Amino acids
Gazeau et al. (2021)
Carbohydrates
Gazeau et al. (2021)
Processes

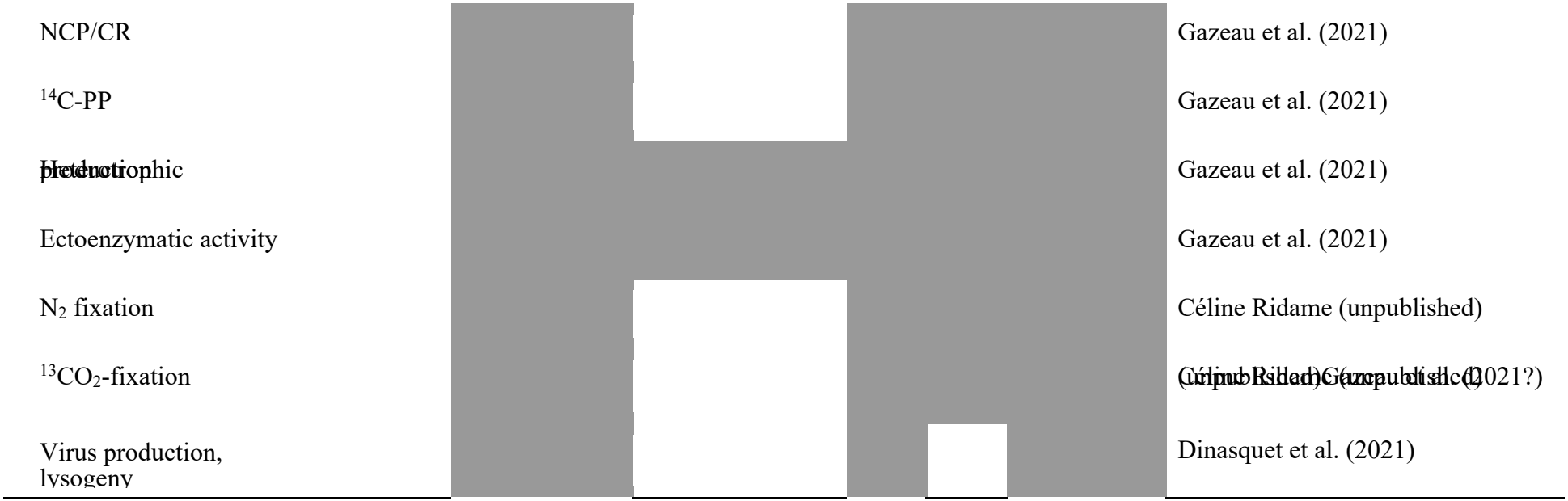
NCP/CR
Gazeau et al. (2021)
^{14}C-PP
Gazeau et al. (2021)
Heterotrophic production
Gazeau et al. (2021)
Ectoenzymatic activity
Gazeau et al. (2021)
N_2 fixation
Céline Ridame (unpublished)
$^{13}CO_2$-fixation
Céline Ridame (unpublished)
Virus production, lysogeny
Dinasquet et al. (2021)

1258

Table 2. Initial conditions as measured while filling the tanks (initial conditions in pumped surface water; sampling time: t-12h). pH_T: pH on the total scale, NO_x: nitrate + nitrite, NH_4: ammonium, DIP: dissolved inorganic phosphorus, $Si(OH)_4$: silicate, TChl*a*: total chlorophyll *a*, HNF: heterotrophic nanoflagellates. The three most important pigments in terms of concentration are also presented (19'-hexanoyloxyfucoxanthin, Zeaxanthin and Divinyl Chlorophyll *a*). Biomasses of the different groups analyzed through flow cytometry were estimated based on conversion equations and/or factors found in the literature (see section 2.3). Autotrophic biomass was, as a first approximation, estimated only based on flow cytometry data and therefore corresponds to the fraction < 20 µm. Heterotrophic biomass was estimated as the sum of heterotrophic prokaryote and HNF biomasses (see section 2.3.2). Values below detection limits are indicated as < dl.

	Sampling station	TYR	ION	FAST
	Coordinates (decimal)	39.34 N, 12.60 E	35.49 N, 19.78 E	37.95 N, 2.90 N
	Bottom depth (m)	3395	3054	2775
	Day and time of sampling (local time)	17/05/2017 17:00	25/05/2017 17:00	02/06/2017 21:00
	Temperature (°C)	20.6	21.2	21.5
	Salinity	37.96	39.02	37.07
Carbonate	pH_T	8.04	8.07	8.03

chemistry	Total alkalinity (µmol kg^{-1})	2529	2627	2443
Nutrients	NO_x (nmol L^{-1})	14.0	18.0	59.0
	NH_4^+ (µmol L^{-1})	0.045	0.022	< dl
	DIP (nmol L^{-1})	17.1	6.5	12.9
	$Si(OH)_4$ (µmol L^{-1})	1.0	0.96	0.64
	NO_x/DIP (molar ratio)	0.8	2.5	4.6
Pigments	TChl*a* (µg L^{-1})	0.063	0.066	0.072
	19'-hexanoyloxyfucoxanthin (µg L^{-1})	0.017	0.021	0.016
	Zeaxanthin (µg L^{-1})	0.009	0.006	0.036
	Divinyl Chlorophyll *a* (µg L^{-1})	~ 0	0	0.014
Flow cytometry	Pico-eukaryotes (abundance in cell mL^{-1}; biomass in µg C L^{-1})	347.8; 0.5	239.9; 0.4	701.0; 1.0
	Nano-eukaryotes (abundance in cell mL^{-1}; biomass in µg C L^{-1})	150.5; 3.9	188.8; 4.8	196.6; 5.0
	Synechococcus (abundance in cell mL^{-1}; biomass in µg C L^{-1})	4972; 1.2	3037; 0.8	6406; 1.6
	Autotrophic biomass (µg C L^{-1})	5.6	6.0	7.7
	Heterotrophic prokaryotes abundance (x 10^5 cell mL^{-1})	4.79	2.14	6.15
	HNF (abundance in cell mL^{-1})	110.1	53.6	126.2
	Heterotrophic biomass (µg C L^{-1})	9.9	4.5	12.7
Microscopy	Pennate diatoms (abundance in cell L^{-1})	140	520	880
	Centric diatoms (abundance in cell L^{-1})	200	380	580

Dinoflagellates (abundance in cell L^{-1})	2770	3000	3410
Autotrophic flagellates (abundance in cell L^{-1})	0	60	650
Ciliates (abundance in cell L^{-1})	270	380	770

1270

Table 3. Maximum input of nitrate + nitrite (NO_x) and dissolved inorganic phosphorus (DIP) released from Saharan dust in tanks D and G as observed from the two discrete samplings performed over the first 6 h after seeding. The estimated maximal percentage of dissolution is also presented (see section 2.3.1 for details on the calculations).

	NO_x				DIP			
	D1	D2	G1	G2	D1	D2	G1	G2
Maximum input			$\mu mol\ L^{-1}$				$nmol\ L^{-1}$	
TYR	11.0	11.1	11.1	11.0	24.6	20.4	24.6	23.9
ION	11.2	11.6	11.2	11.3	23.3	22.0	19.6	22.9
FAST	11.3	11.1	11.1	11.2	30.8	31.3	36.9	29.8
Percentage of dissolution (%)								
TYR	95	96	95	94	12	10	12	11
ION	96	99	96	97	11	10	9	11
FAST	97	97	95	97	15	15	17	14

Table 4. Removal rate of nitrate + nitrite (NO_x) and dissolved inorganic phosphorus (DIP) in tanks D and G during the three experiments (TYR, ION and FAST). For NO_x, decreasing rates were estimated based on linear regressions between maximal concentrations (i.e. after dust enrichment, at t1h or t6h) and final concentrations (t72 h for TYR and ION and t96h for FAST). For DIP, decreasing rates were estimated based on linear regressions between maximal concentrations (i.e. after dust enrichment at t1h or t6h) and concentrations measured at sampling times after which a stabilization was observed. This sampling time is shown in parentheses. All rates are expressed in nmol L^{-1} h^{-1}.

	NO_x			DIP		
	TYR	ION	FAST	TYR	ION	FAST
D1	-6.5	-8.6	-14.3	-0.4 (t72h)	-0.5 (t48h)	-0.2 (t96h)
D2	-1.0	-8.6	-13.5	-0.3 (t72h)	-0.8 (t24h)	-0.2 (t96h)
G1	-6.7	-13.1	-21.6	-1.3 (t24h)	-0.8 (t24h)	-1.5 (t24h)
G2	-0.8	-1.6	-25.2	-1.3 (t24h)	-1.6 (t24h)	-1.1 (t24h)

Table 5. Maximum relative changes in tanks D and G as compared to controls (average between C1 and C2), expressed as a %, for the three experiments (TYR, ION and FAST). The sampling time at which these maximum relative changes were observed is shown in brackets. Tchl*a* refers to the concentration of total chlorophyll *a* and B_{micro} to the biomass proxy of micro-phytoplankton (sum of Fucoxanthin and Peridinin, see Material and Methods) based on high performance liquid chromatography (HPLC). HP and HNF refer to heterotrophic prokaryote and heterotrophic nanoflagellate abundances, respectively, as measured by flow cytometry.

Experiment	Tank	HPLC		Flow cytometry				
		TChl*a*	B_{micro}	Pico-eukaryotes	Nano-eukaryotes	*Synechococcus*	HP	HNF
TYR	D1	-35 (t24h)	-33 (t12h)	-75 (t72h)	-80 (t1h)	-71 (t48h)	68 (t72h)	352 (t72h)
TYR	D2	-38 (t12h)	-39 (t24h)	-75 (t72h)	-80 (t1h)	-72 (t48h)	53 (t72h)	100 (t72h)
TYR	G1	60 (t72h)	52 (t72h)	-75 (t1h)	89 (t72h)	76 (t72h)	67 (t72h)	1095 (t72h)
TYR	G2	359 (t72h)	392 (t72h)	323 (t72h)	119 (t72h)	700 (t72h)	68 (t48h)	298 (t72h)
ION	D1	183 (t72h)	157 (t72h)	126 (t72h)	89 (t72h)	317 (t72h)	128 (t72h)	44 (t72h)
ION	D2	109 (t72h)	156 (t72h)	117 (t72h)	-59 (t1h)	390 (t72h)	133 (t72h)	27 (t72h)
ION	G1	399 (t72h)	454 (t72h)	458 (t72h)	256 (t72h)	805 (t72h)	176 (t72h)	175 (t72h)

ION	G2	426 (t72h)	612 (t72h)	510 (t72h)	292 (t72h)	1425 (t72h)	161 (t72h)	129 (t72h)
FAST	D1	318 (t96h)	356 (t96h)	113 (t96h)	208 (t72h)	348 (t96h)	27 (t96h)	-38 (t96h)
FAST	D2	237 (t96h)	322 (t96h)	91 (t96h)	219 (t72h)	197 (t96h)	40 (t48h)	-49 (t96h)
FAST	G1	399 (t96h)	415 (t96h)	198 (t72h)	274 (t72h)	357 (t48h)	61 (t48h)	243 (t24h)
FAST	G2	395 (t96h)	421 (t96h)	129 (t72h)	202 (t96h)	344 (t48h)	67 (t48h)	74 (t24h)

Figure captions

Fig. 1. Location of the sampling stations in the Mediterranean Sea onboard the R/V "Pourquoi Pas ?" during the PEACETIME cruise, on map of satellite-derived surface chlorophyll *a* concentration averaged over the entire duration of the cruise (Courtesy of Louise Rousselet).

Fig. 2. Scheme of an experimental tank (climate reactor).

Fig. 3. Proportion of the different pigments, as measured by high performance liquid chromatography (HPLC) in pumped surface seawater for the three experiments (t-12h).

Fig. 4. Continuous measurements of temperature and irradiance level (PAR) in the six tanks during the three experiments. The dashed vertical line indicates the time of dust seeding (after t0).

Fig. 5. pH on the total scale (pH_T) and total alkalinity (A_T) measured in the six tanks during the three experiments. The dashed vertical line indicates the time of dust seeding (after t0). Error bars correspond to the standard deviation based on analytical triplicates.

Fig. 6. Nutrients (nitrate + nitrite: NO_x, dissolved inorganic phosphorus: DIP, silicate: $Si(OH)_4$ as well as the molar ratio between NO_x and DIP, measured in the six tanks during the three experiments. The dashed vertical line indicates the time of seeding (after t0).

Fig. 7. Concentrations of total chlorophyll *a* and major pigments, measured by high performance liquid chromatography (HPLC), in the six tanks during the three experiments. The dashed vertical line indicates the time of seeding (after t0).

Fig. 8. Abundance of autotrophic pico-eukaryotes, autotrophic nano-eukaryotes, *Synechococcus,* heterotrophic prokaryotes (HP), and heterotrophic nano-flagellates (HNF), measured by flow cytometry, in the six tanks during the three experiments. The evolution of autotrophic biomass

(see Material and Methods for details on the calculation) is also shown. The dashed vertical line indicates the time of seeding (after t0).

Fig. 9. Abundances of meso-zooplankton species as measured at the end of each experiment.

Fig. 10. Maximal relative change (%) of main biological stocks (TCHl*a*: total chlorophyll *a*, HP: heterotrophic prokaryotes) and processes (BP: bacterial production; PP: ^{14}C-based primary production; see Gazeau et al., 2021; BR: bacterial respiration (no data from this study); and N_2 fixation, Céline Ridame, unpublished results) as obtained during the present study at the 3 stations (TYR, ION and FAST) under ambient conditions of pH and temperature (open red squares) and future conditions (full green squares). Squares are delimited by the range of responses observed among the duplicates for each treatment. The dotted green squares for station TYR denote the large variability observed between duplicates for some parameters and processes that prevented drawing solid conclusions. Box-plots represent the distribution of responses observed from studies conducted in the Mediterranean Sea, as compiled by Guieu and Ridame (2020).

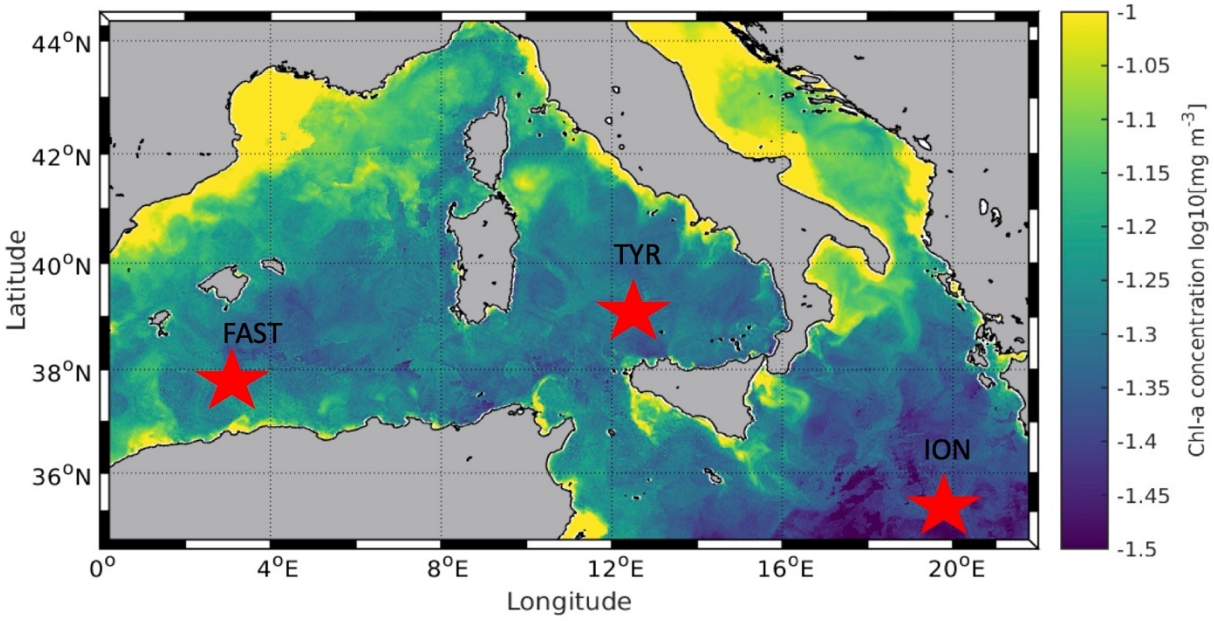
44°N
42°N
40°N
38°N
36°N
Latitude
0°
4°E
8°E
12°E
16°E
20°E
Longitude
FAST
TYR
ION
-1
-1.05
-1.1
-1.15
-1.2
-1.25
-1.3
-1.35
-1.4
-1.45
-1.5
Chl-a concentration log10[mg m-3]

Fig. 1.

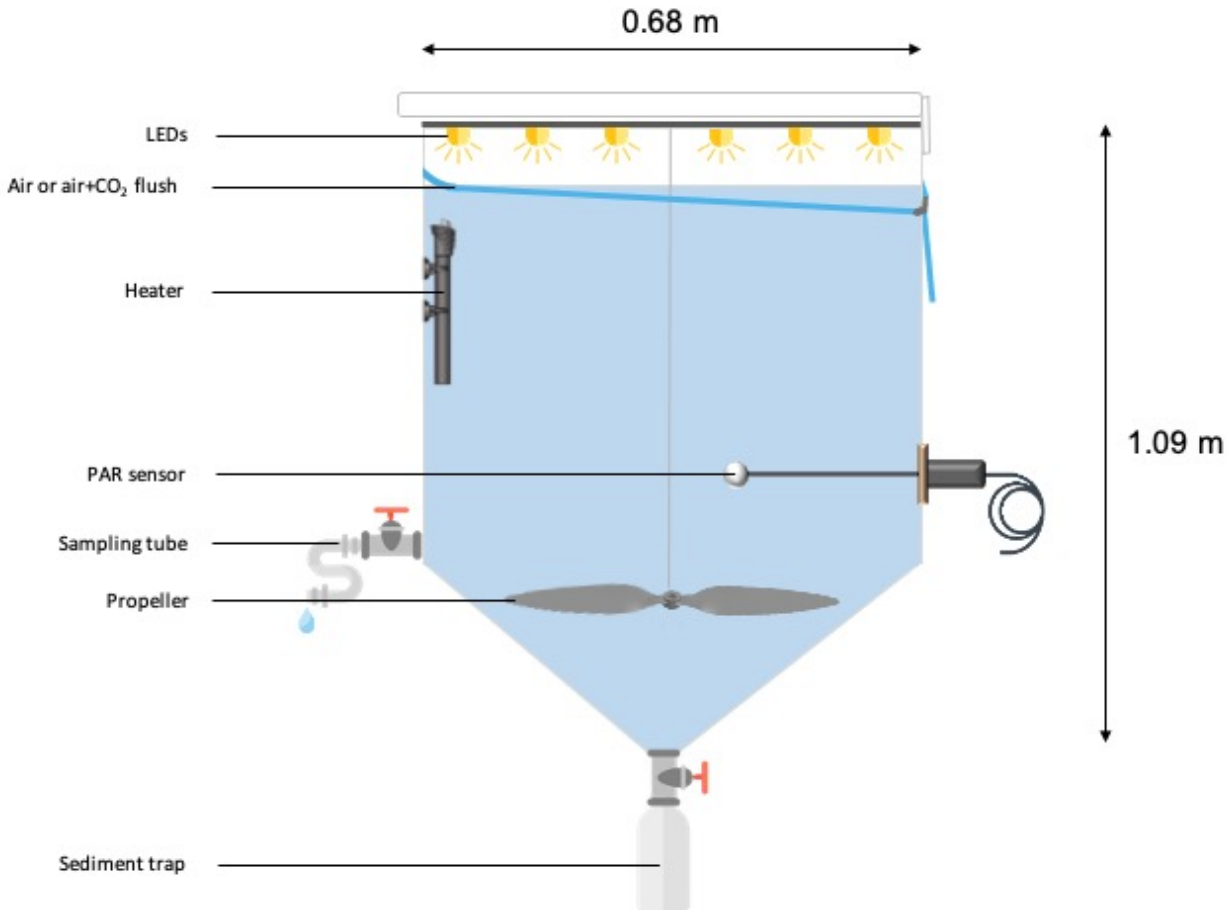
0.68 m
LEDs
Air or air+CO_2 flush
Heater
PAR sensor
Sampling tube
Propeller
Sediment trap
1.09 m

Fig. 2.

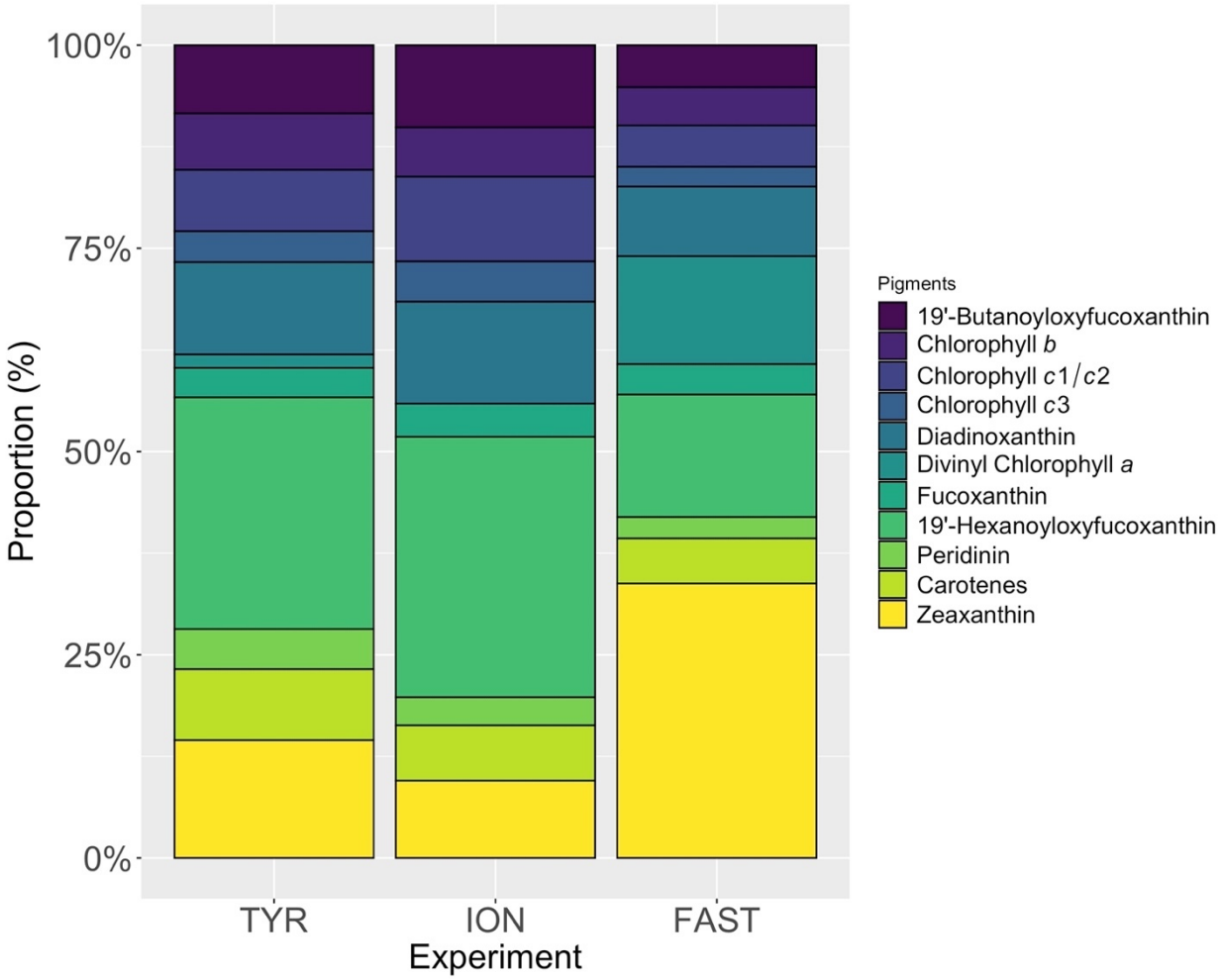
100%
75%
50%
25%
0%
Proportion (%)
TYR
ION
FAST
Experiment
Pigments
19'-Butanoyloxyfucoxanthin
Chlorophyll b
Chlorophyll c1/c2
Chlorophyll c3
Diadinoxanthin
Divinyl Chlorophyll a
Fucoxanthin
19'-Hexanoyloxyfucoxanthin
Peridinin
Carotenes
Zeaxanthin

Fig. 3.

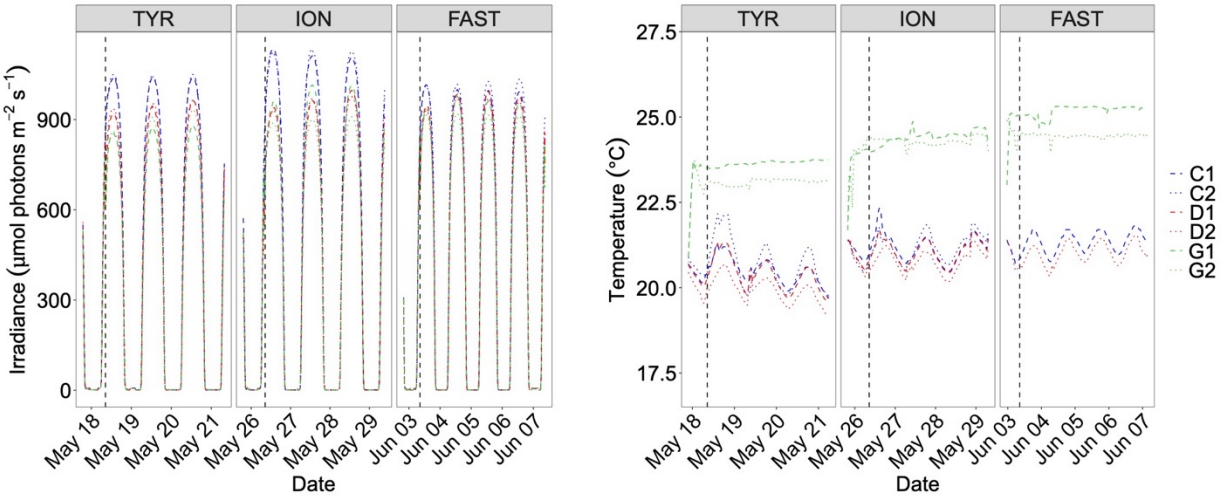
TYR
ION
FAST
Irradiance (µmol photons m^{-2} s^{-1})
0
300
600
900
May 18
May 19
May 20
May 21
May 26
May 27
May 28
May 29
Jun 03
Jun 04
Jun 05
Jun 06
Jun 07
Date
Temperature (°C)
17.5
20.0
22.5
25.0
27.5
C1
C2
D1
D2
G1
G2

Fig. 4.

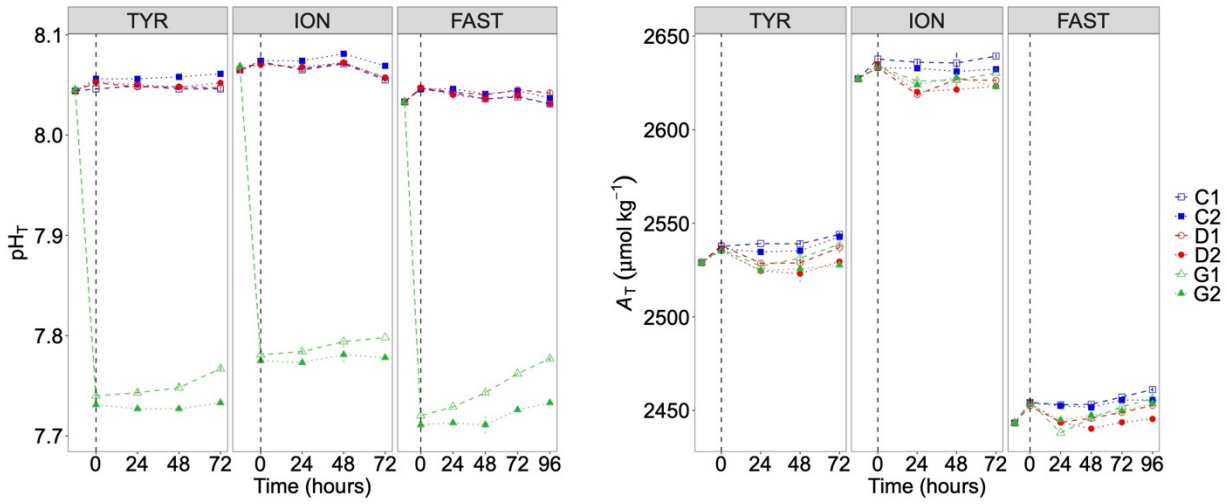
TYR
ION
FAST
8.1
8.0
7.9
7.8
7.7
pH_T
0 24 48 72
0 24 48 72
0 24 48 72 96
Time (hours)
2650
2600
2550
2500
2450
A_T (µmol kg^-1)
0 24 48 72
0 24 48 72
0 24 48 72 96
Time (hours)
C1
C2
D1
D2
G1
G2

Fig. 5.

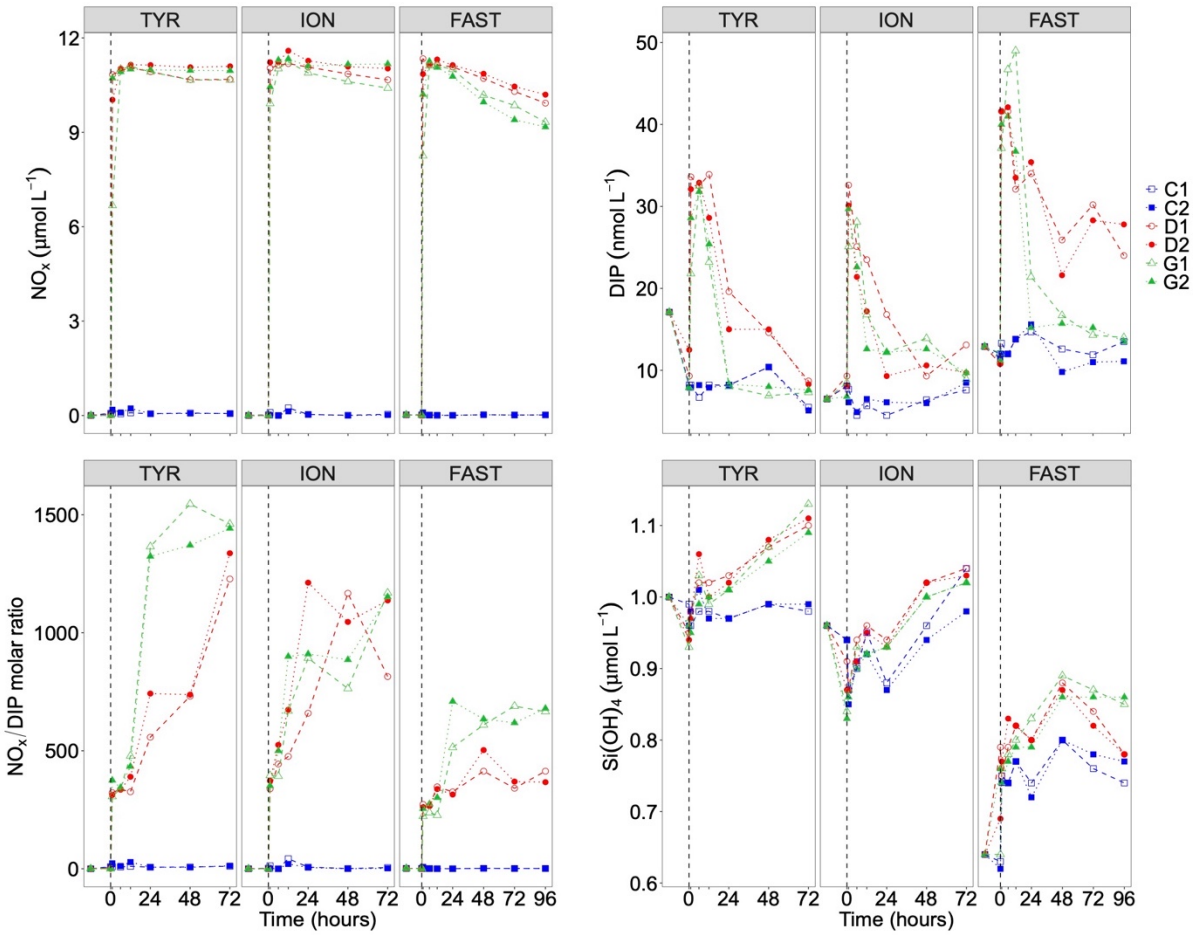
TYR
ION
FAST
NOx (µmol L−1)
DIP (nmol L−1)
NOx/DIP molar ratio
Si(OH)4 (µmol L−1)
Time (hours)
C1
C2
D1
D2
G1
G2

Fig. 6.

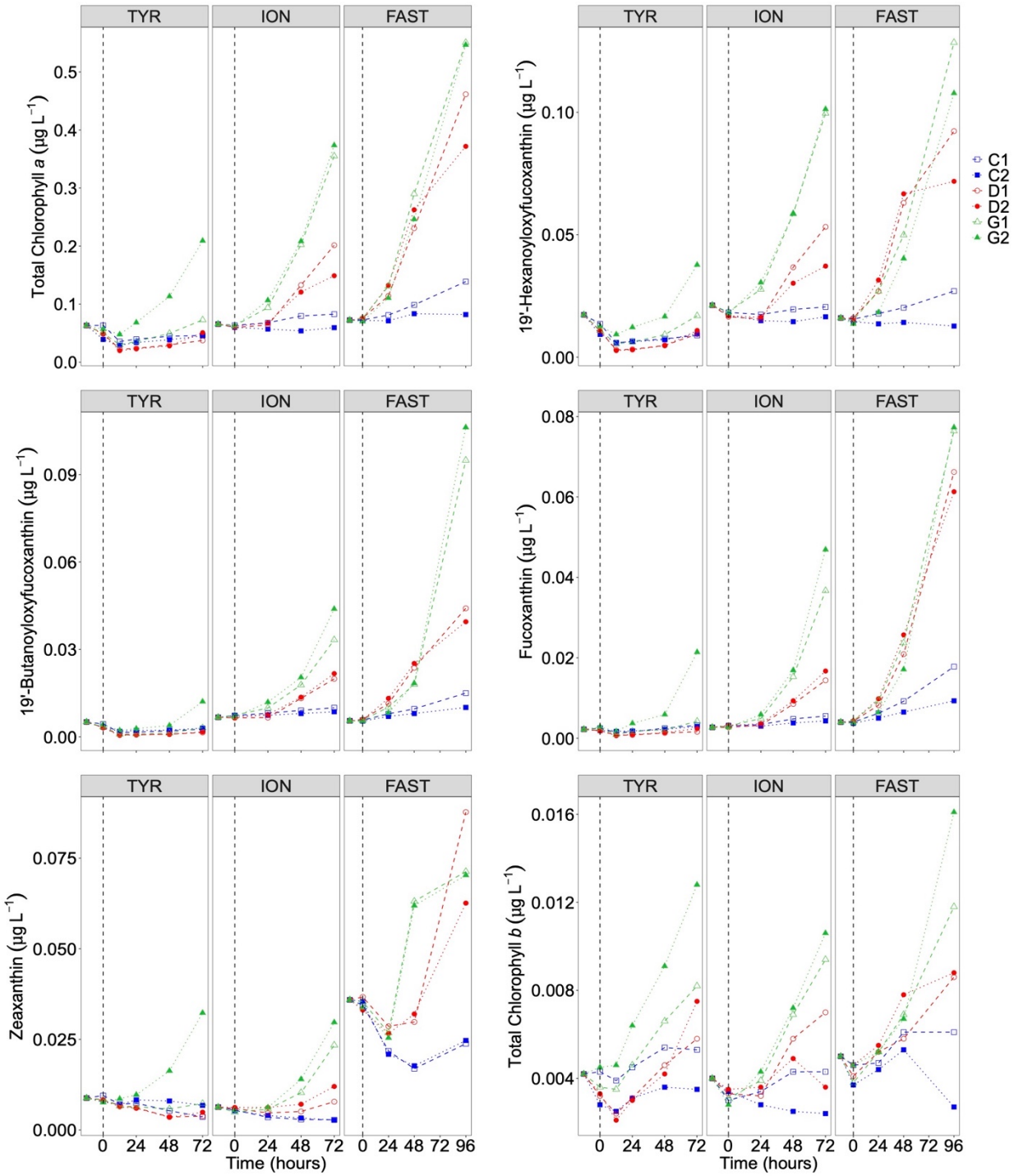
TYR
ION
FAST
Total Chlorophyll a (µg L⁻¹)
19'-Hexanoyloxyfucoxanthin (µg L⁻¹)
19'-Butanoyloxyfucoxanthin (µg L⁻¹)
Fucoxanthin (µg L⁻¹)
Zeaxanthin (µg L⁻¹)
Total Chlorophyll b (µg L⁻¹)
Time (hours)
C1
C2
D1
D2
G1
G2

Fig. 7.

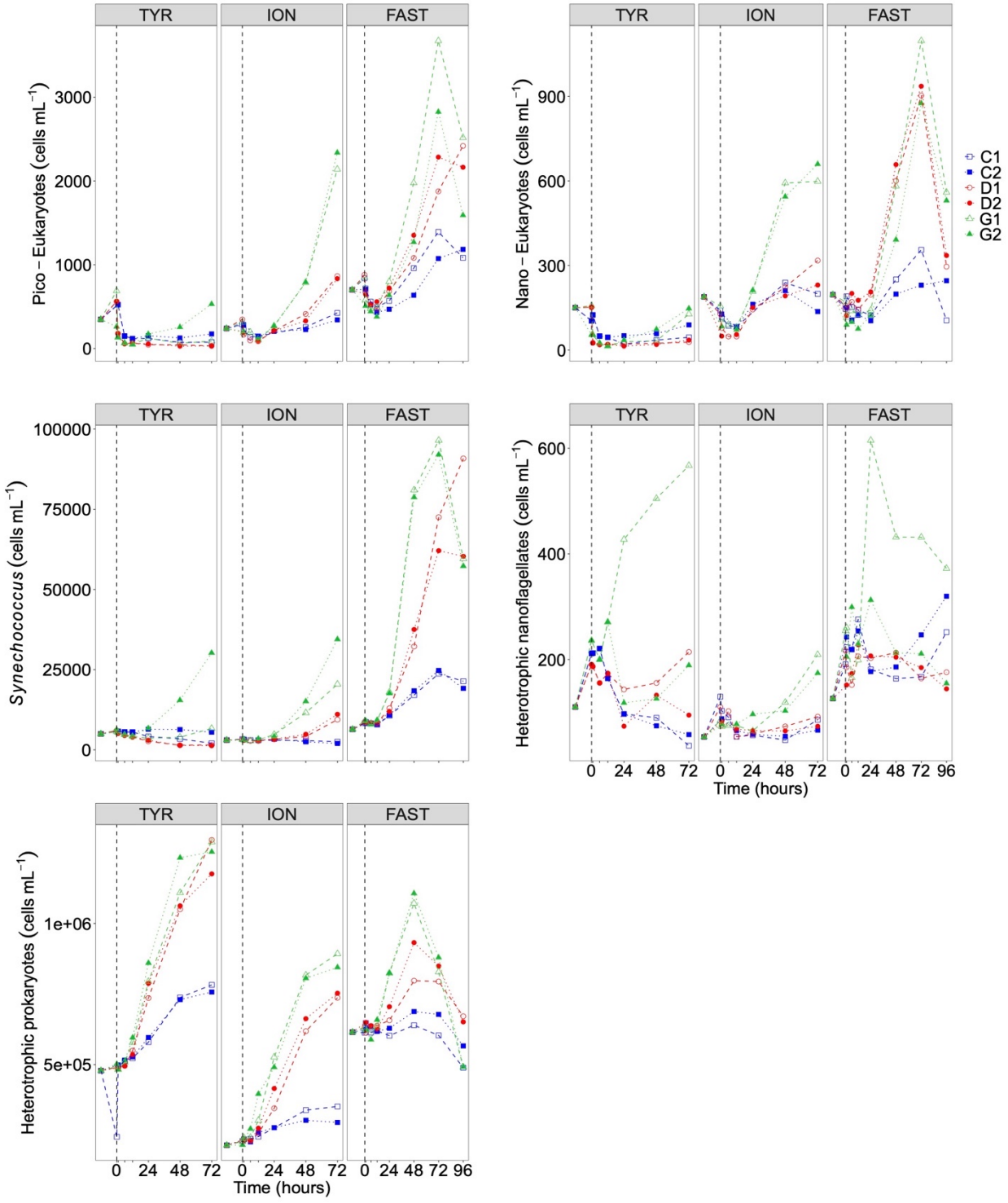
TYR
ION
FAST
Pico – Eukaryotes (cells mL^{-1})
Nano – Eukaryotes (cells mL^{-1})
Synechococcus (cells mL^{-1})
Heterotrophic nanoflagellates (cells mL^{-1})
Heterotrophic prokaryotes (cells mL^{-1})
C1
C2
D1
D2
G1
G2
Time (hours)

Fig. 8.

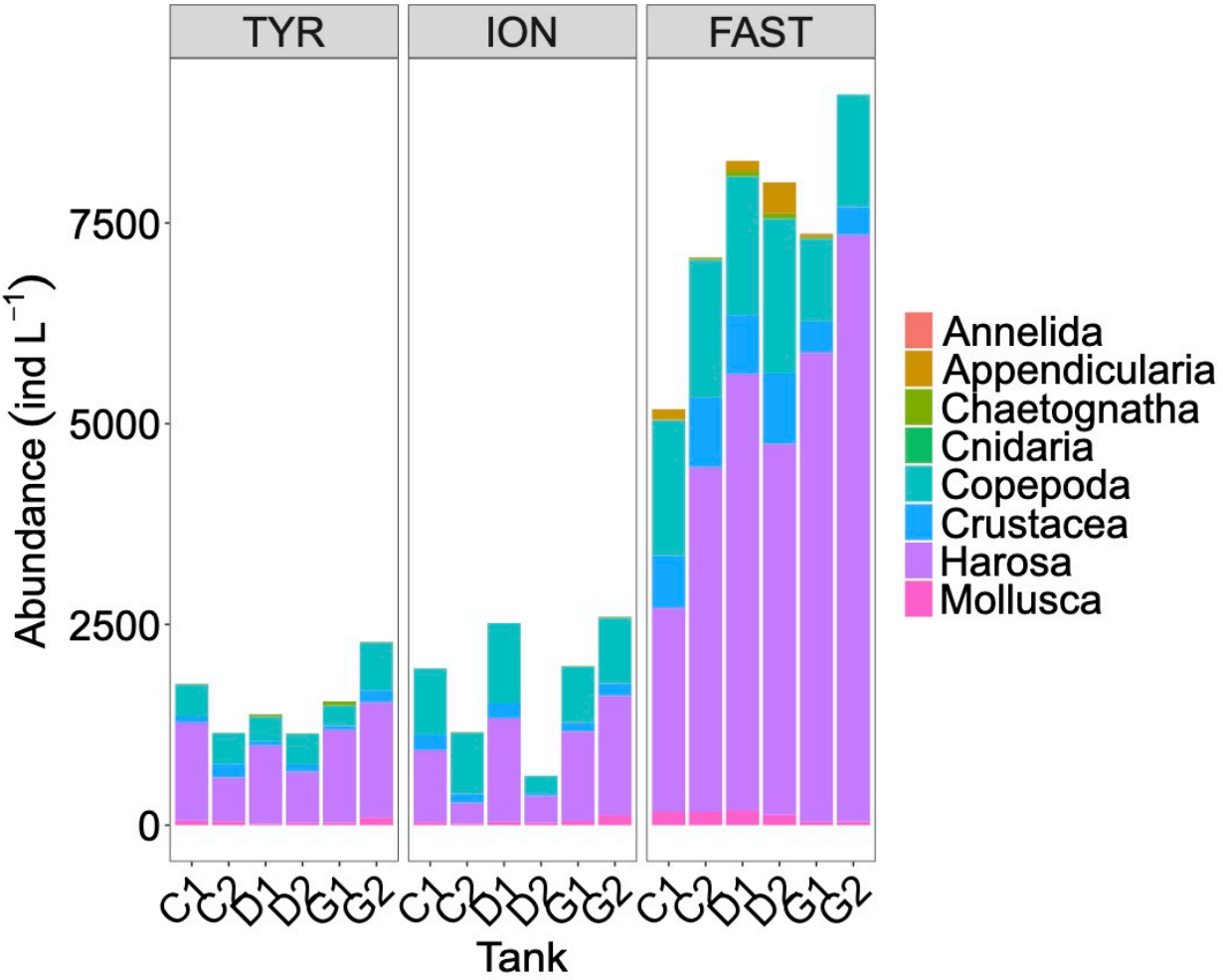
TYR
ION
FAST
7500
5000
2500
0
Abundance (ind L^{-1})
Annelida
Appendicularia
Chaetognatha
Cnidaria
Copepoda
Crustacea
Harosa
Mollusca
Tank

Fig. 9.

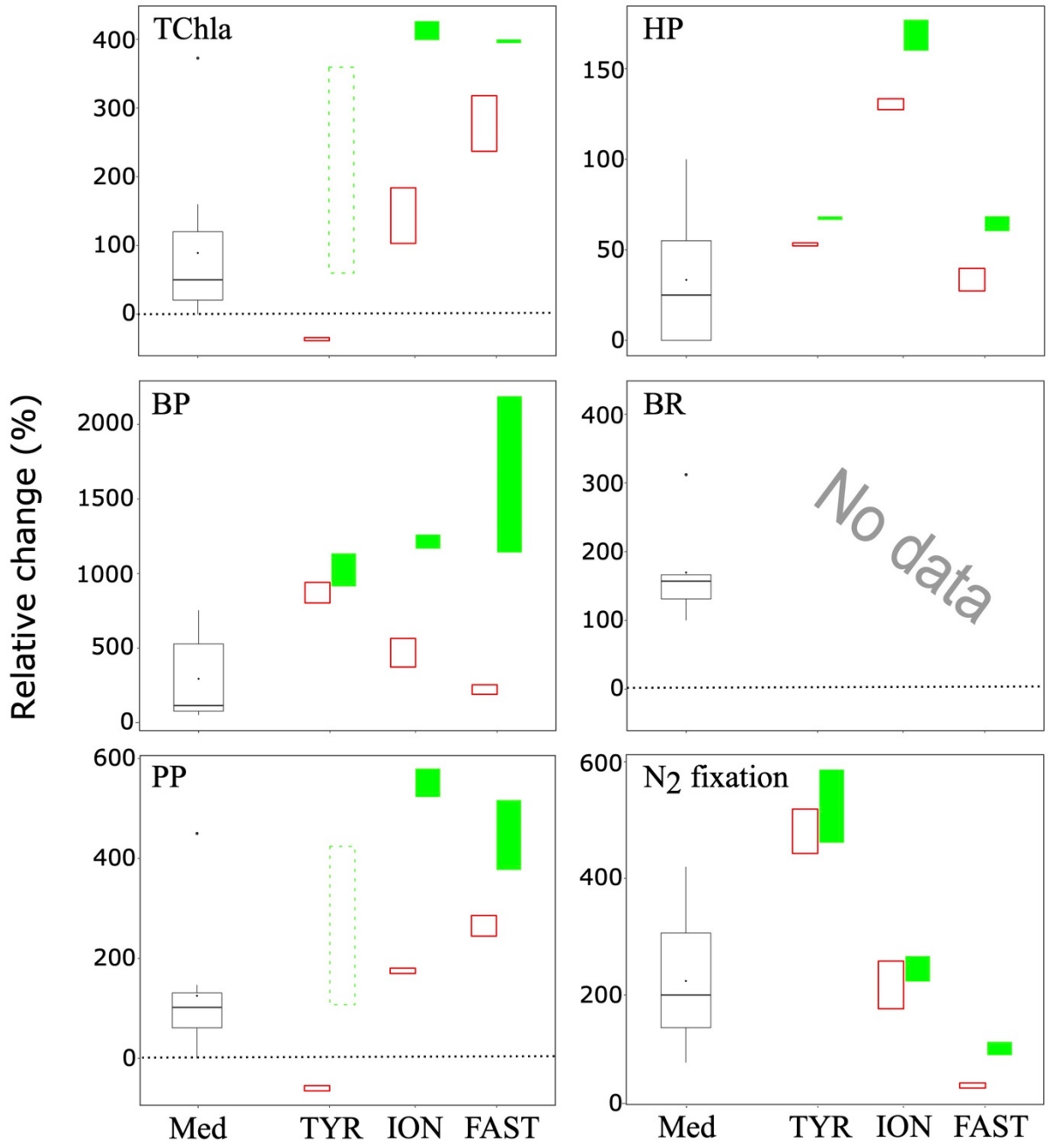
TChla
HP
BP
BR
No data
PP
N2 fixation
Relative change (%)
Med
TYR
ION
FAST

Fig. 10.